Supporting Information

NiMoFe nanoparticles@MoO_2 nano-pillar arrays as bifunctional electrodes for ultra-low-voltage overall water splitting

Peng Liu, [a] Weisheng Pan, [a] Rui Yao,[a] Lihan Zhang,[a] Qianyuan Wu,[b] Feiyu Kang,[a] Hong Jin Fan,[c] Cheng Yang*[a]

[a] Institute of Materials Research, Tsinghua Shenzhen International Graduate School, Tsinghua University, Shenzhen 518055, China

[b] Institute of Environment Ecology, Tsinghua Shenzhen International Graduate School, Tsinghua University, Shenzhen 518055, China

[c] School of Physical and Mathematical Sciences, Nanyang Technological University, Singapore 637371, Singapore

*E-mail: yang.cheng@sz.tsinghua.edu.cn

Preparation of NiMo(Fe) NPs@MoO_2 NPAs and other multielement NPs@MoO_2 NPAs.

The NiMoFe NPs@MoO_2 NPAs were fabricated by a two-step process. First, the precursors were prepared by a hydrothermal method. A commercial nickel foam (1 x 3 cm^2, thickness: 1.5 mm, bulk density: 0.19 g cm^{-3}) was selected as the substrate. Before hydrothermal reaction, the nickel foam was first sonicated in ethanol and 5.0 M HCl solution for 5 min to remove the organic impurities and NiO_x layer on the surface, respectively, rinsed subsequently with deionized water (DI water) and then dried in air. A piece of NF and 15 mL aqueous solutions containing $Ni(NO_3)_2$ ($6H_2O$) (0.233 g), $(NH_4)_6Mo_7O_{24}$ (0.233 g) and $FeCl_2$ (0~0.1 g) were put into a stainless reactor which was heated to 150 °C for a 6-hour hydrothermal reaction. All solutions in the experiments were prepared with analytical grade chemicals and DI water. $FeCl_2$ used for 2-5# sample were 0.01, 0.025, 0.05 and 0.1g, respectively. Second, the as-synthesized precursors were dried in the air and annealed in the H_2/Ar (v/v, 5/95) atmosphere at 500 °C for 2 h to obtain the NiMo(Fe) NPs@MoO_2 NPAs. The average mass loading of the as-obtained Ni_xFe_{1-x}-NCAs was about 35-40 mg cm^{-2}. The NiMoCo, NiMoRu, CoMoFe and

NiMoCoFe NPs@MoO_2 NPAs were prepared by the same process as preparing the NiMoFe NPs@MoO_2 except adopting a certain amount of $RuCl_3$ and $Co(NO_3)_2$ ($6H_2O$). The pure MoO_2 nano pillar arrays on NF were prepared by etching the NiMo nanoparticles away from the NiMo NPs@MoO_2 NPAs using 3M HCl solution**.**

Fabrication of Pt/C-NF and IrO_2-NF electrodes. To prepare the Pt/C-NF electrodes, 20 mg commercial Pt/C, 100 μL Nafion, 100 μL ethanol and 500 μL deionized water were ultrasonicated for 20 min to obtain a homogeneous dispersion. Then, a piece of clean nickel foam was dipped into the dispersion, which was then dried in the air at 60 °C for 4 h. The mass loading of Pt/C catalyst on nickel foam was controlled to be ~ 4 mg cm^{-2}**.** To prepare the IrO_2-NF electrodes, 80 mg IrO_2, 200 μL Nafion, 500 μL isopropanol and 400 μL deionized water were ultrasonicated for 30 min to obtain a homogeneous dispersion. Then, a piece of clean nickel foam was dipped into the dispersion, which was then dried in the air at 60 ºC for 4 h. The mass loading of the IrO_2 catalyst on nickel foam was controlled to be ~ 16 mg cm^{-2}.

Materials characterizations. The micromorphology and energy dispersive X-Ray spectroscopy (EDS) of catalysts was characterized by field emission scanning electron microscopy (FE-SEM, SAPPHIRE SUPRA 55). The high-resolution transmission electron microscope (HRTEM) images and Energy Dispersive Spectrometry (EDS) of catalysts were obtained by JEOL ARM 200F and JEOL JEM-3200FS, Japan. Crystallographic information was obtained with X-ray diffraction (Bruker DSRINT2000/PC, Germany) using Cu Kα radiation with λ=1.5418 Å (at a diffraction angle ranging from 10° to 80° at a scan rate of 5°/min). Raman spectra of the materials were obtained with a spectrometer (Lab RAM HR spectrometer, Horiba, Japan) operating with argon-ion laser (532 nm) as the excitation light source. X-ray photoelectron spectra (XPS) were measured with Al-Kα radiation (50 W, 15 kV) (ESCALABSB 250 Xi). The shift of binding energy due to relative surface charging was corrected using the C 1 s level at 284.6 eV as an internal standard. The contact angles of water

and gas bubbles under electrolyte were tested by the method of captive bubble using the Kruss DSA30 system. Composition analyses of Ni, Fe and Mo contained in the nanoparticles were obtained from the SPECTRO ARCOS II MV inductively coupled plasma optical emission spectrometer (ICP-OES, Germany). The powder of the sample was soaked in the concentrated hydrochloric acid for 3 minutes to ensure enough dissolution of metallic nanoparticles and avoid the dissolution of the MoO_2 substrate.

Electrochemical measurements. Electrochemical measurements were conducted with the electrochemical working station (CHI 660E) in a three-electrode electrochemical setup. A 1 M KOH solution was used as the electrolyte, and a Hg/HgO electrode (in 1 M KOH) and graphite rod (with a diameter of 8 mm) were used as a reference and counter electrodes, respectively. The as-prepared electrodes supported on Ni foam were utilized as the working electrode. The working area was tailored to 0.4 cm^2. To convert the measured potential versus the Hg/HgO electrode into the potential versus reversible hydrogen electrode (RHE), the Hg/HgO reference electrode was calibrated using RHE in 1 M KOH solution. Testing equipment was shown in Figure S9a. The Pt and graphite were employed as working electrode (WE) and counter electrode (CE) in 1 M KOH electrolyte. The electrolyte was saturated by hydrogen via bubbling hydrogen in the buttom of the electrolyser firstly. Then continuous H_2 was blown over the surface of the electrolyte to keep a H_2-saturated environment when collecting data. To perform the calibration, a series of CV measurements were carried out to determine the zero current potential (the interconversion between the hydrogen oxidation and hydrogen evolution reaction). The scan rate of the CV measurement is set as low as 1 mV S^{-1} to avoid the possible contribution of capacitive current. As shown in Figure S9b, the result shows that the potential of zero net current can be estimated at -0.924 V versus the Hg/HgO electrode, and the relation between the Hg/HgO reference and RHE in 1 M KOH solution can thus be established using formula $E_{RHE} = E_{Hg/HgO} + 0.924$ V in 1 M KOH solution.

iR compensation was performed by the automatic current interrupt method with a value of 93% x Ru for OER and 95% x Ru for HER through the CHI 660E working station. For OER, in order to provide reliable electrochemical data and avoid overlap between Ni^{2+}/Ni^{3+} oxidation and OER, polarization curves were recorded from high initial potentials to low final potentials with a 5 mV s^{-1} scan rate. Tafel slopes were calculated using the polarization curves by plotting overpotential against log (current density). Chronopotentiometry measurements were performed to evaluate the long-term stability. ECSA was determined by measuring the capacitive current associated with double-layer charging from the scan-rate dependence of CVs. For this, the potential window of CVs was 0.1-0.2 V versus Hg/HgO. The scan rates were 100, 200, 300, 400 and 500 mV s^{-1}. The double-layer capacitance (C_{dl}) was estimated by plotting the $\Delta j = (ja\text{-}jc)$ at 0.15 V versus Hg/HgO against the scan rate. The linear slope is twice of the double layer capacity. The ECSA values were calculated from the measured double layer capacitance divided by the specific capacitance of an atomically smooth material (C_{dl}', ~40 μF cm^{-2}): ECSA = $C_{dl} \div C_{dl}' \times S$, where S is the actual surface area of the electrode. The electrochemical impedance spectroscopies (EIS) measurement was conducted at 1.53 V (vs. RHE) for OER and -0.1 V (vs. RHE) for HER, in the frequency range from100 kHz to 0.01 Hz with an amplitude of 5 mV. The tests of full water splitting were conducted by a two-electrode electrochemical setup by combining the countering electrode and reference electrode with 95% iR compensation. The R_u used for iR compensation for the chronopotentiometry test were obtained from the EIS tests at 0 V vs. Hg/HgO.

Numerical simulation methods. All the spin-polarized density functional theory (DFT) calculations were performed by using Vienna Ab-initio Simulation Package[1] (VASP) under the Projected Augmented Wave[2] (PAW) method. The revised Perdew-Burke-Ernzerhof (RPBE) functional was used to describe the exchange and correlation effects.[3] In all the

calculations, the cutoff energy was set to be 450 eV. The (111) surface was simulated to represent the catalytic interface. The slab model was constructed by six atomic layer with 4×4 supercell. The Monkhorst-Pack grids[4] were set to be 2×2×1 for computing the surface calculations. A 15 Å vacuum layer was applied in z-direction of the slab models, preventing the slabs from vertical interactions.

In alkaline conditions, HER could occur via the following elementary steps:

$H_2O + * \rightarrow *OH + *H$

$*H \rightarrow * + ½H_2\uparrow$

where * denotes the active sites on the catalyst surface. The free energy of the adsorbed hydrogen is defined as:

$$\Delta G_{H^*} = \Delta E_H + \Delta E_{ZPE} - T\Delta S_H$$

where ΔE_H is the hydrogen binding energy, ΔE_{ZPE} is the zero point energy difference between adsorbed hydrogen and gaseous hydrogen, and $T\Delta S$ is the corresponding entropy difference between these two states.

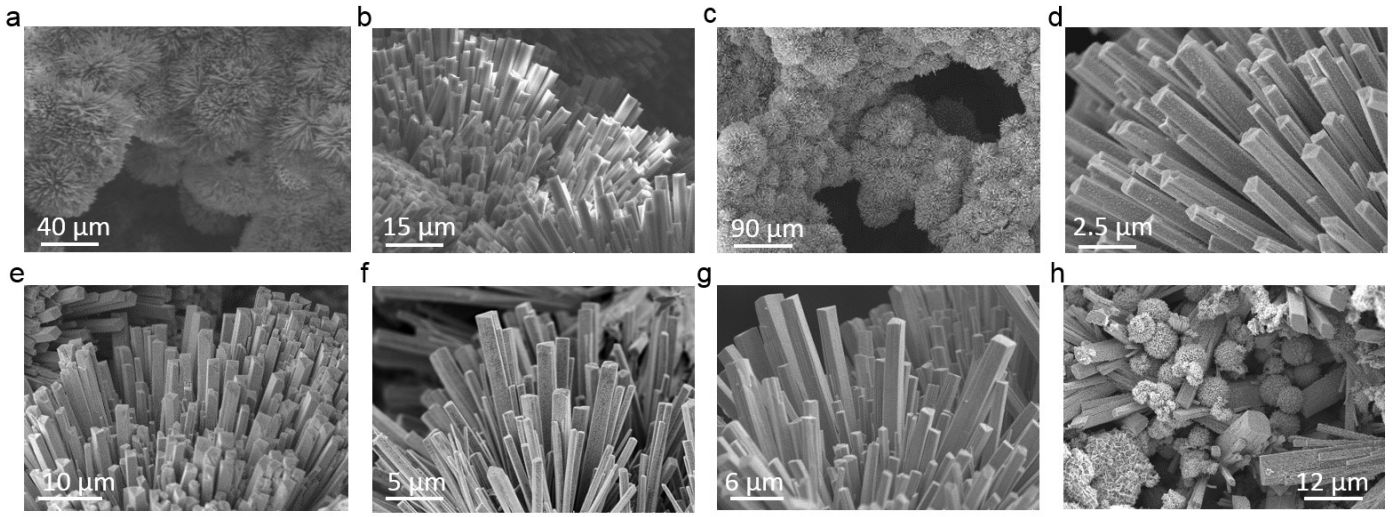

Figure S1. SEM images of the precursor (a-b) and a corresponding annealed sample (c-d) of 1# NiMoFe NPs@MoO_2 NPAs. SEM images of annealed samples of (e) 2#, (f) 3#, (g) 4# and (h) 5# NiMoFe NPs@MoO_2 NPAs are also provided.

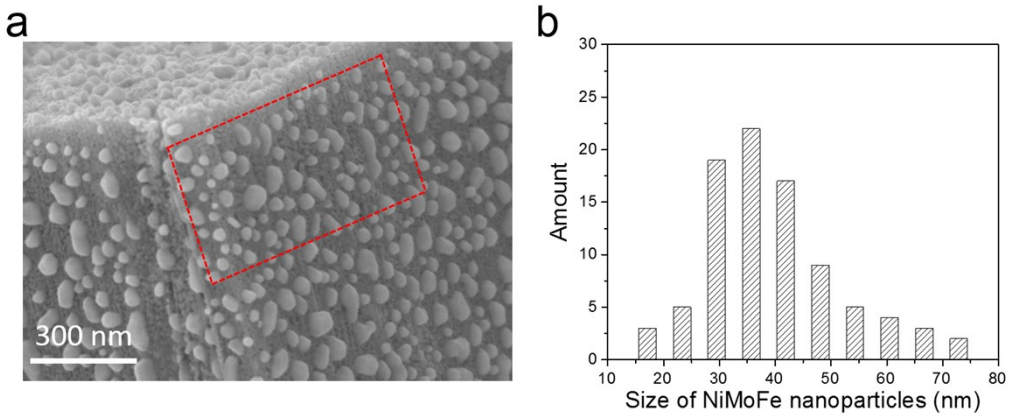

Figure S2. (a) SEM images of an annealed sample of 4# NiMoFe NPs@MoO_2 NPAs. (b) Size distribution of the nanoparticles on 4# sample measured from (a). The density of the nanoparticle is calculated from the area surrounded by a red parallelogram in (a).

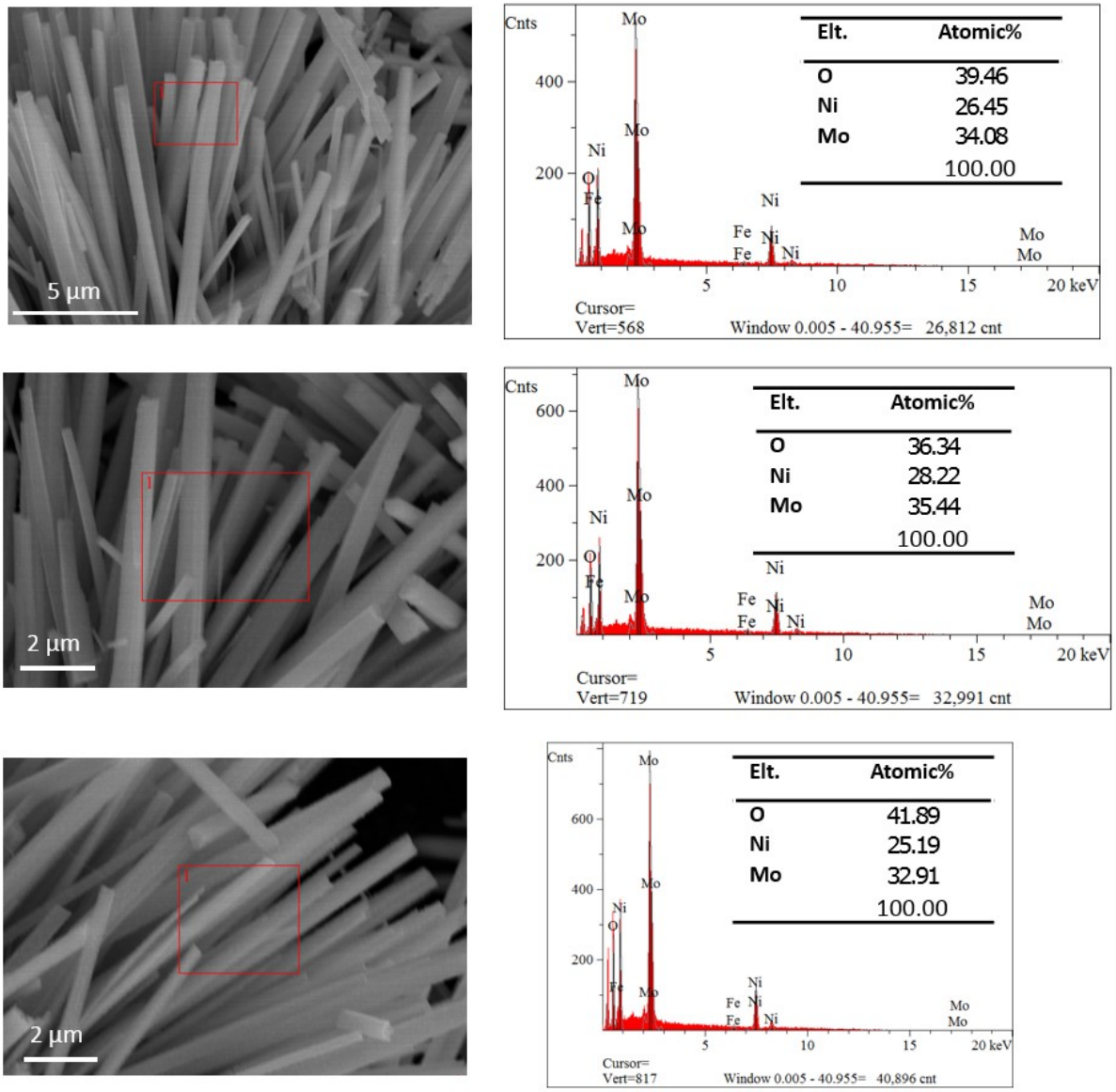

Figure S3a. SEM images and corresponding EDS quantitative analysis of 1# sample of NiMo NPs@MoO_2 NPAs.

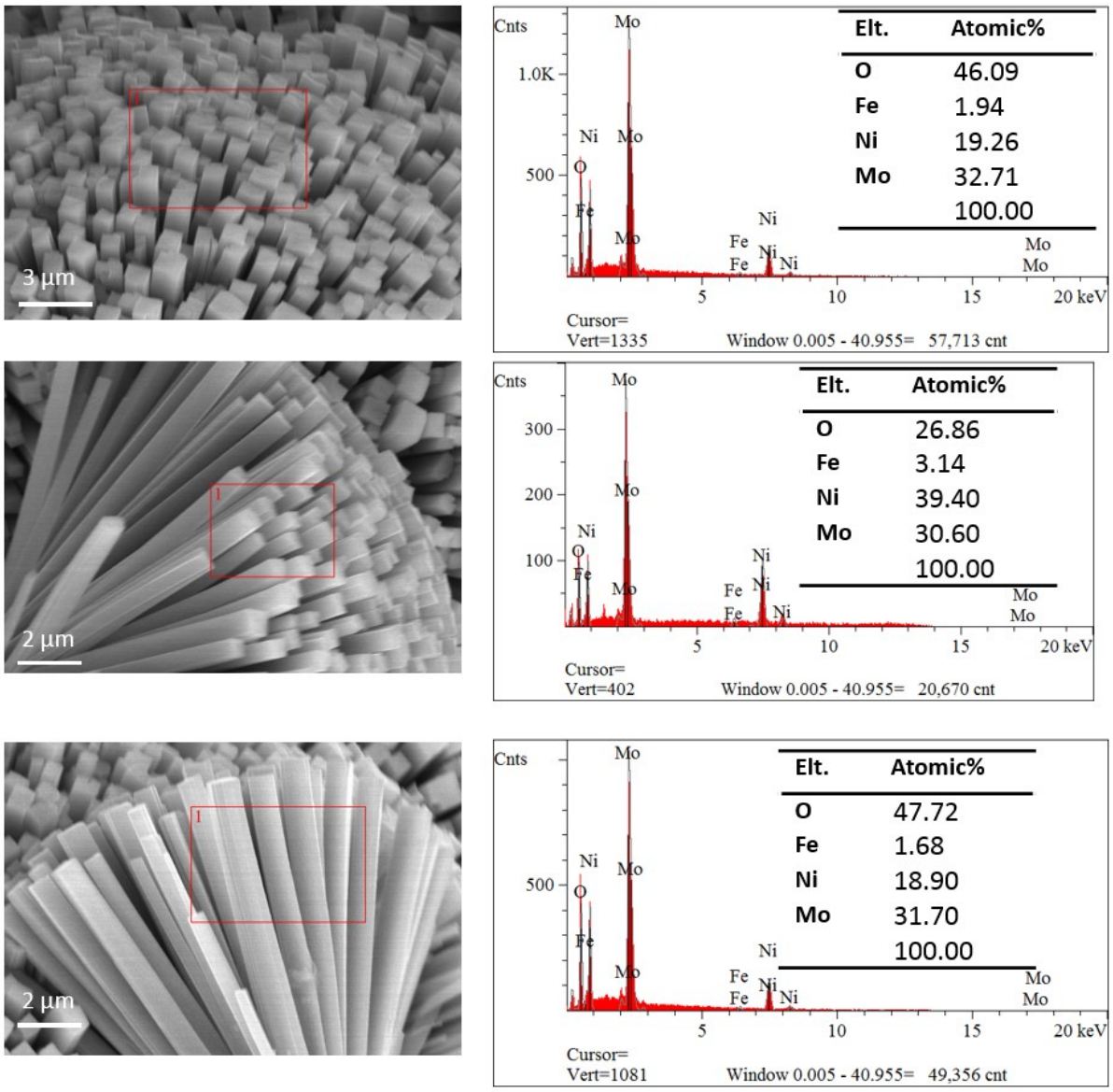

Figure S3b. SEM images and corresponding EDS quantitative analysis of 2# sample of NiMoFe NPs@MoO_2 NPAs.

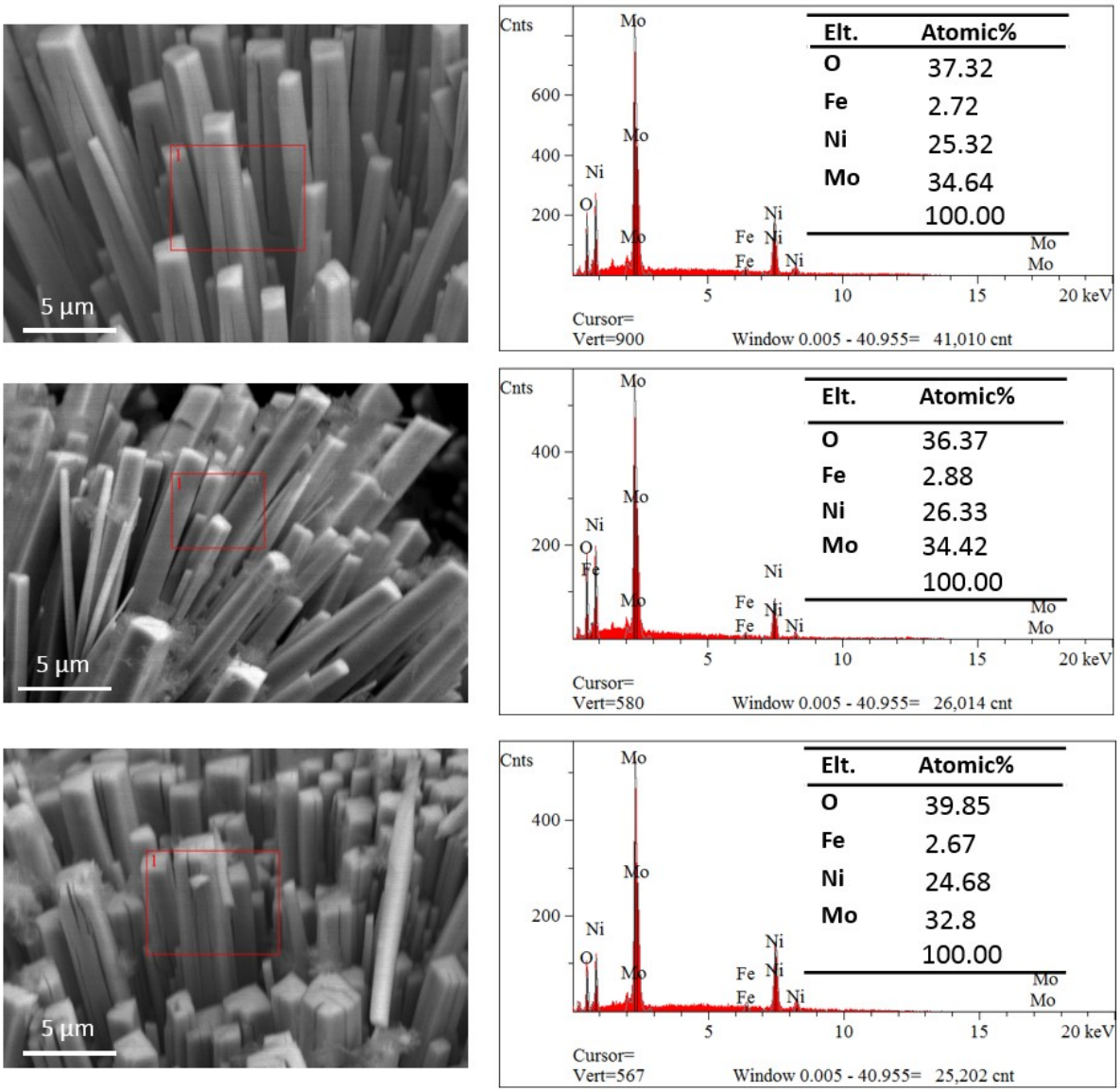

Figure S3c. SEM images and corresponding EDS quantitative analysis of 3# sample of NiMoFe NPs@MoO_2 NPAs.

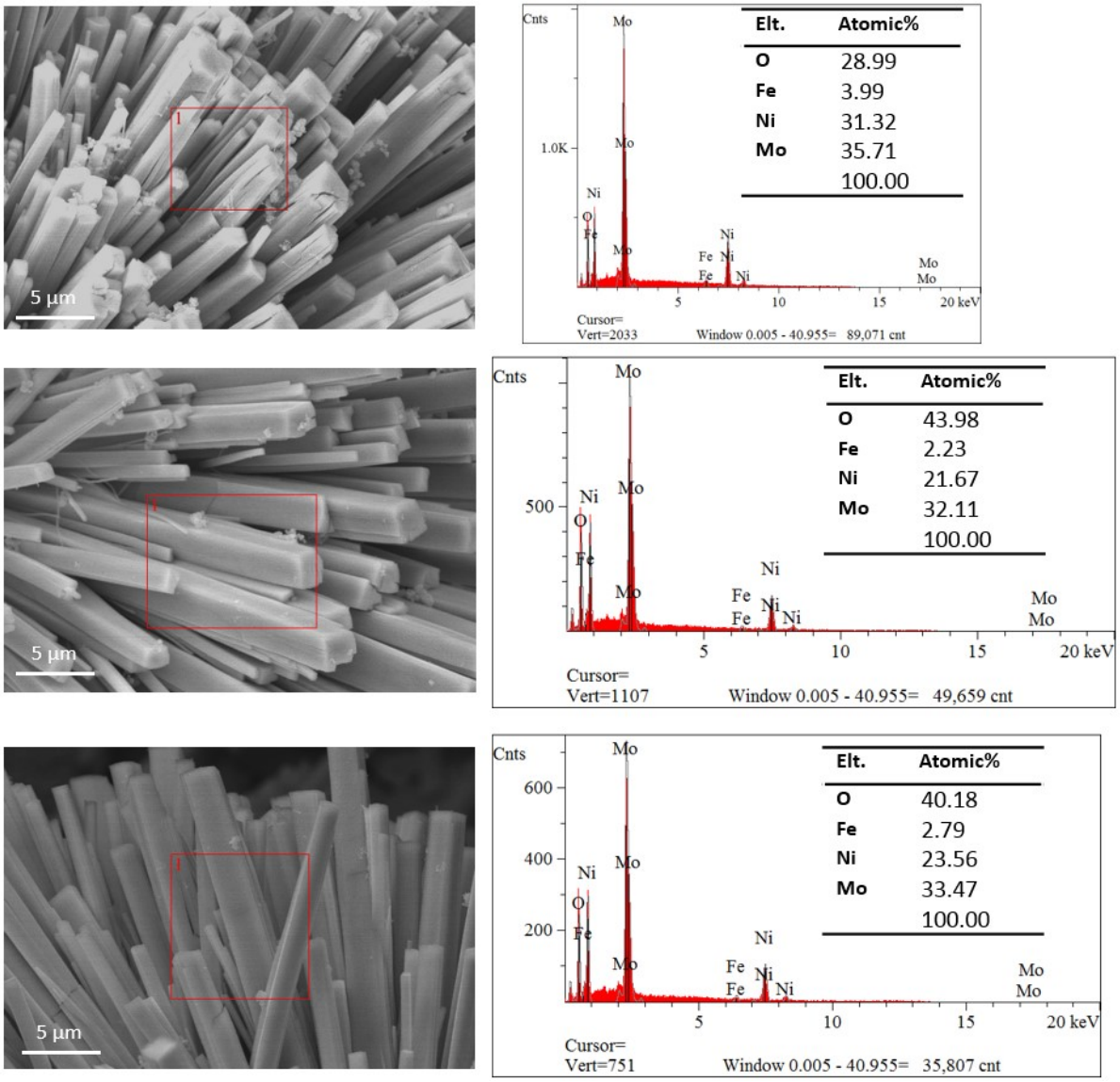

Figure S3d. SEM images and corresponding EDS quantitative analysis of 4# sample of NiMoFe NPs@MoO_2 NPAs.

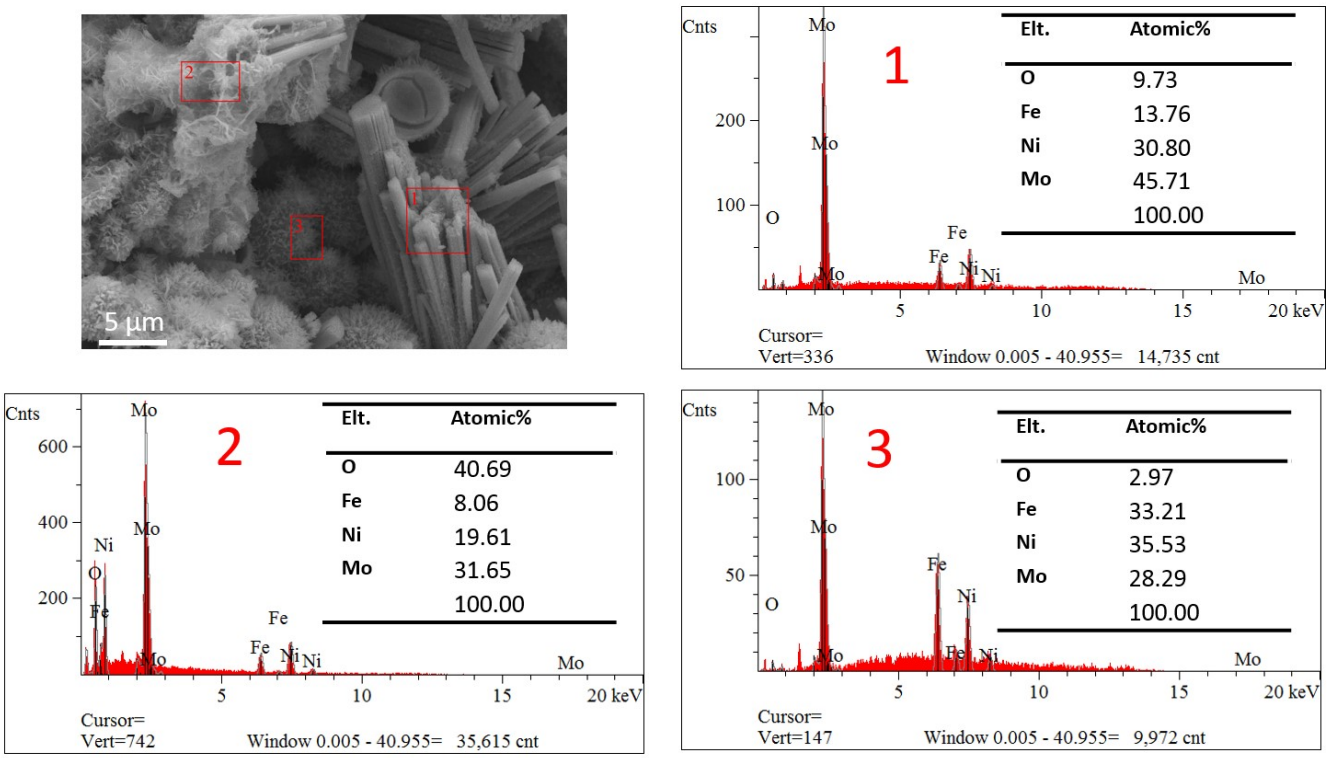

Figure S3e. SEM images and corresponding EDS quantitative analysis of 5# sample of NiMoFe NPs@MoO_2 NPAs.

Table S1. Summary of compositions (at%) of 1-5# sample of NiMo(Fe) NPs@MoO_2 NPAs from SEM EDS.

Element	1#	2#	3#	4#	5#
O	39.2	40.2	37.8	37.7	17.8
Fe	0.0	2.3	2.8	3.0	18.3
Ni	26.7	25.9	25.4	25.5	28.6
Mo	34.1	31.7	34.0	33.8	35.2

Table S2. Summary of compositions (at%) of 1-5# NiMo(Fe) NPs@MoO_2 NPAs from ICP-OES.

Element	1#	2#	3#	4#	5#
Fe	0.0	0.1	1.8	3.9	14.9
Mo	22.6	24.3	27.3	25.2	31.3
Ni	77.4	75.6	70.9	70.9	53.8

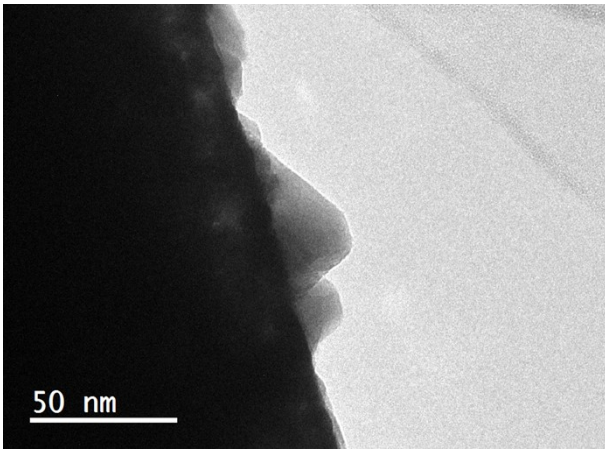

Figure S4. TEM image of the annealed 4# sample of NiMoFe NPs@MoO_2 NPAs.

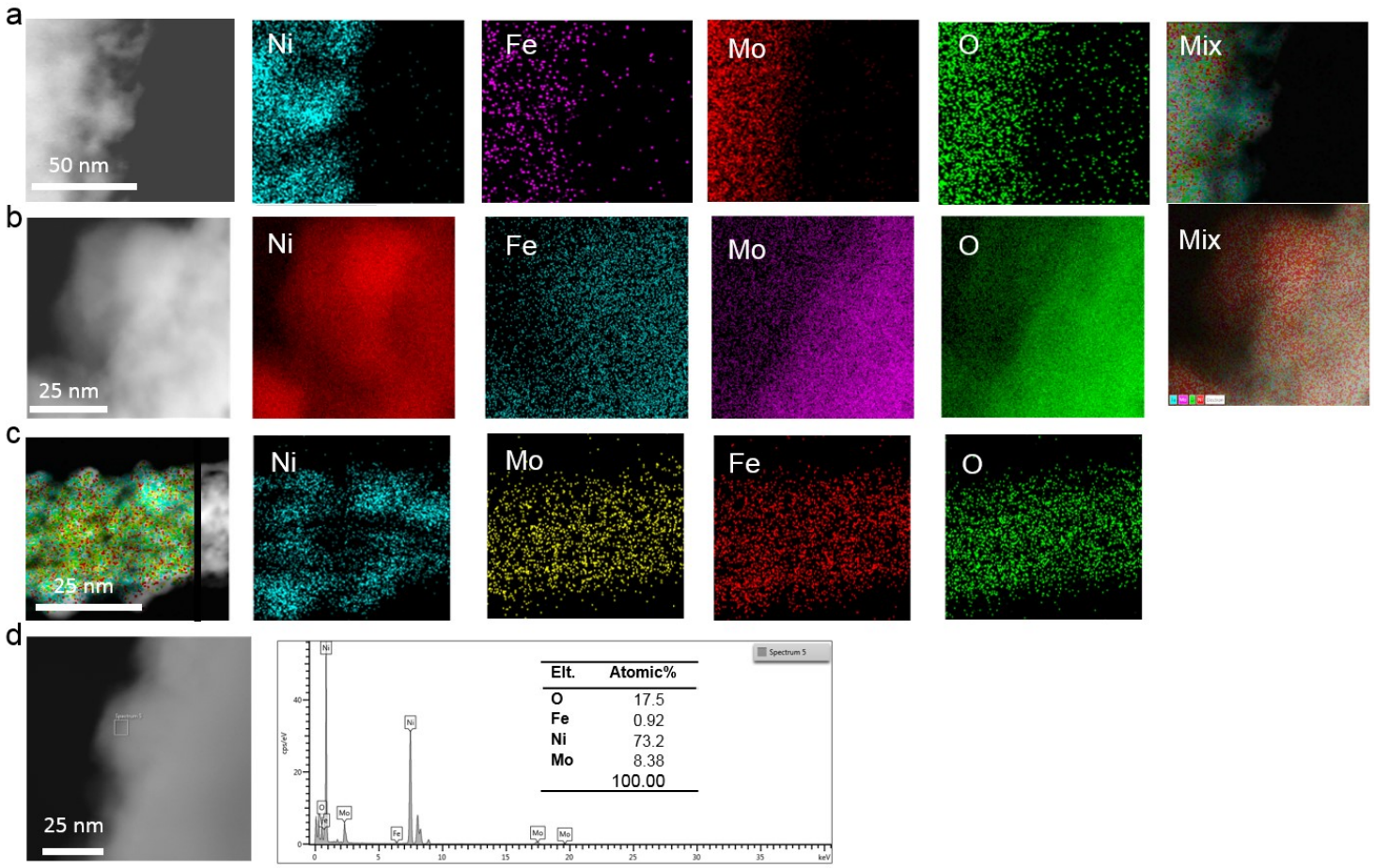

Figure S5. (a-c) TEM image of 4# NiMoFe NPs@MoO_2 NPAs and corresponding EDS mapping images of Ni, Fe, Mo, O and their mixture. (d) TEM selected area EDS quantitative analysis.

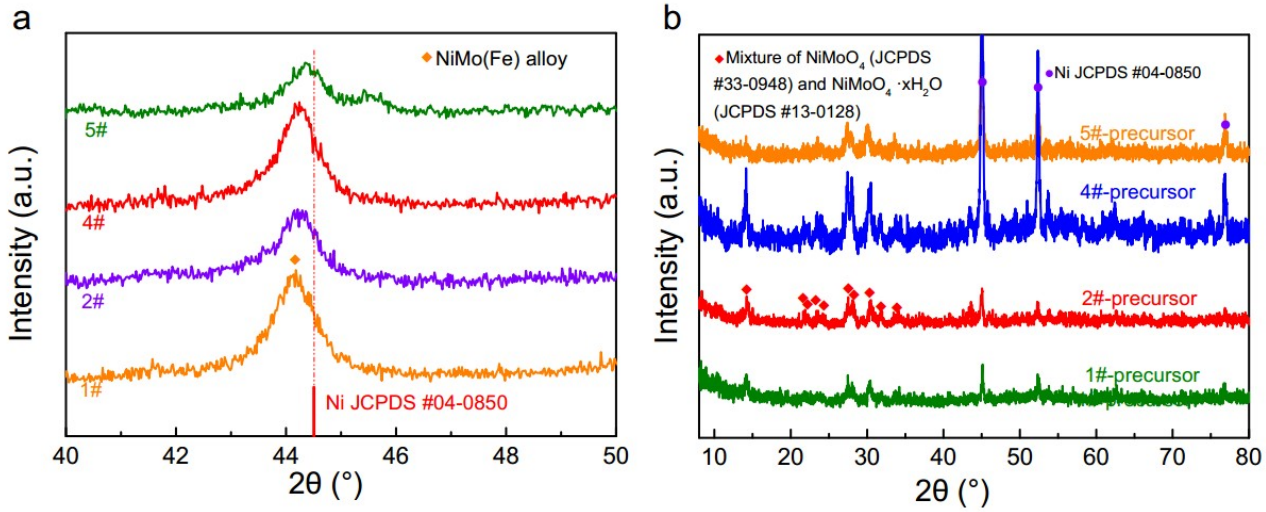

Figure S6. (a) Local magnification of XRD patterns of 1-2 and 4-5# NiMo(Fe) NPs@MoO_2 NPAs in Figure 2a. (b) XRD patterns of the precursors of 1-2 and 4-5# samples on NF.

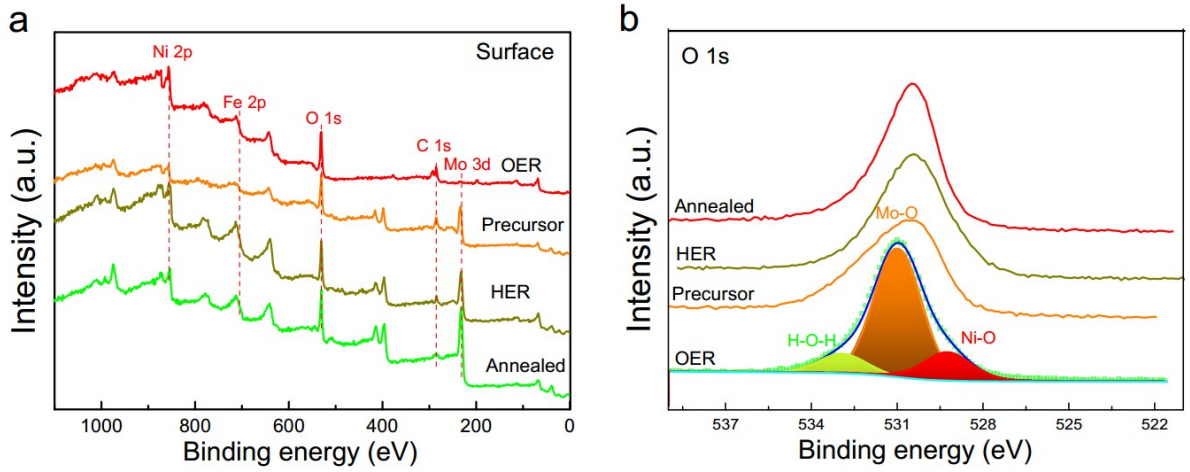

Figure S7. (a) Wide-scanning XPS spectra of as-prepared 4# NiMoFe NPs@MoO_2 NPAs and (b) O 1s fine spectrum of the samples after long-term OER tests.

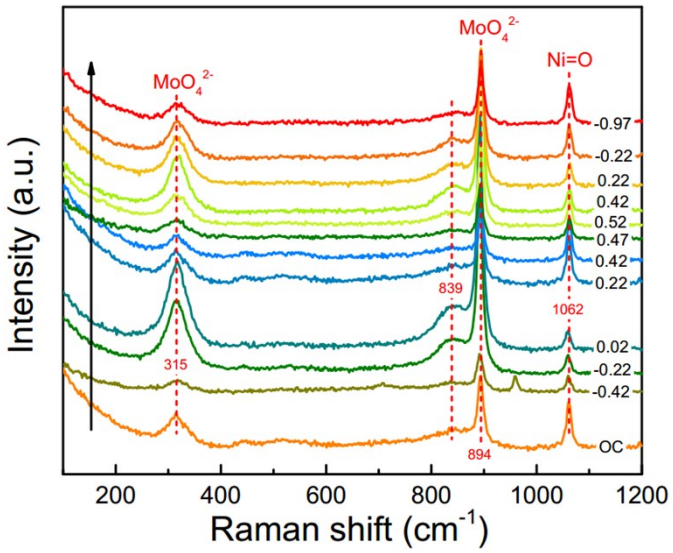

Figure S8. *in situ* Raman spectra of 4# NiMoFe NPs@MoO_2 NPAs precursor under different potentials.

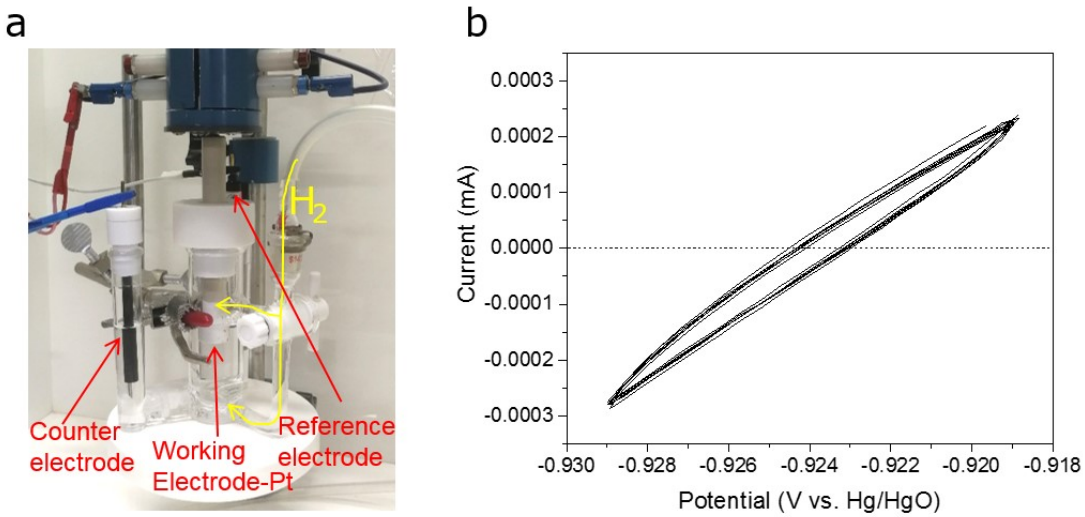

Figure S9. Calibration of Hg/HgO reference electrode with respect to RHE. (a) Testing equipment. (b) CV curves of Pt electrode under H_2-saturated 1M KOH electrolyte.

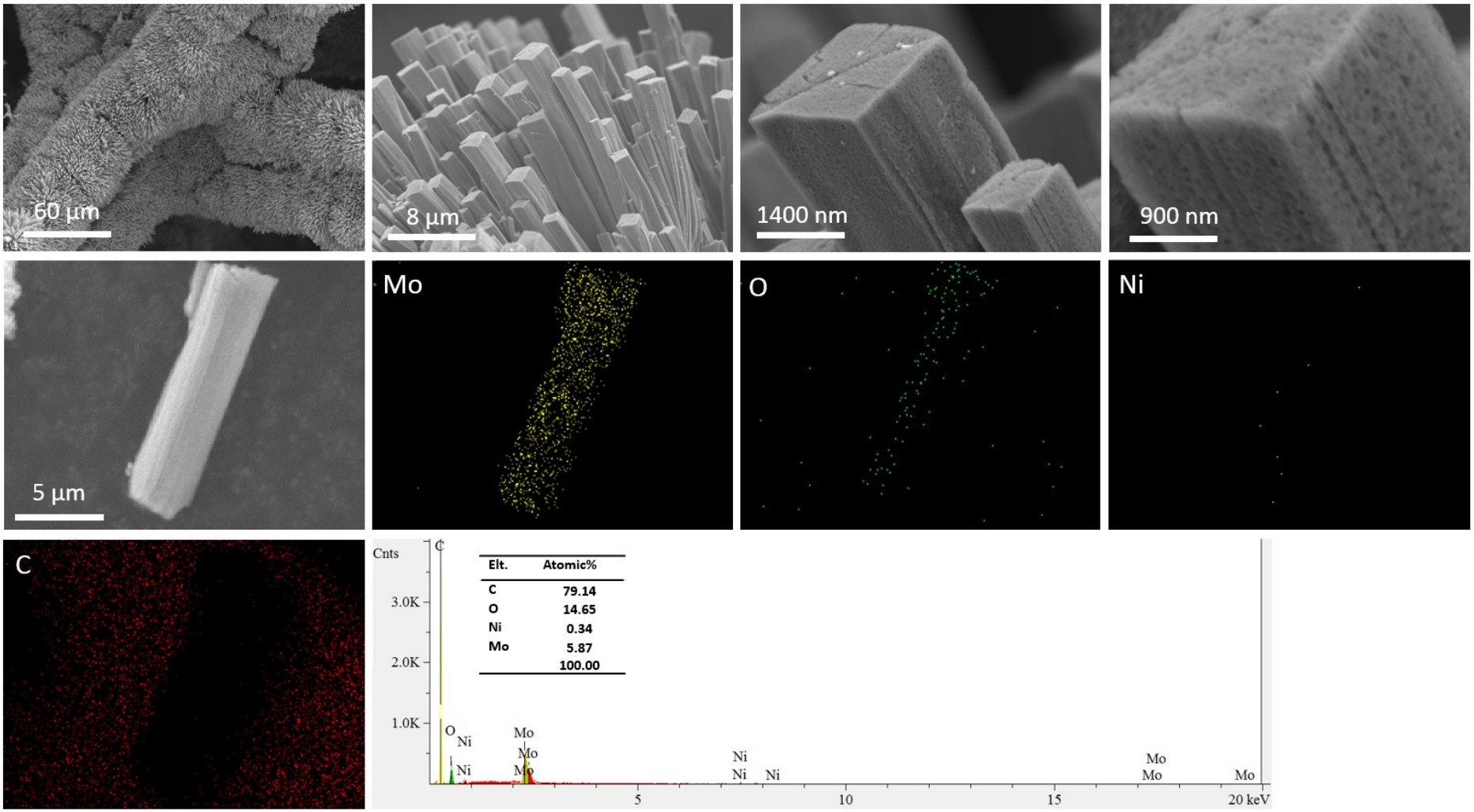

Figure S10. SEM images and corresponding EDS analysis of pure MoO_2 nano pillar arrays (acid etched 1# sample of NiMo NPs@MoO_2 NPAs).

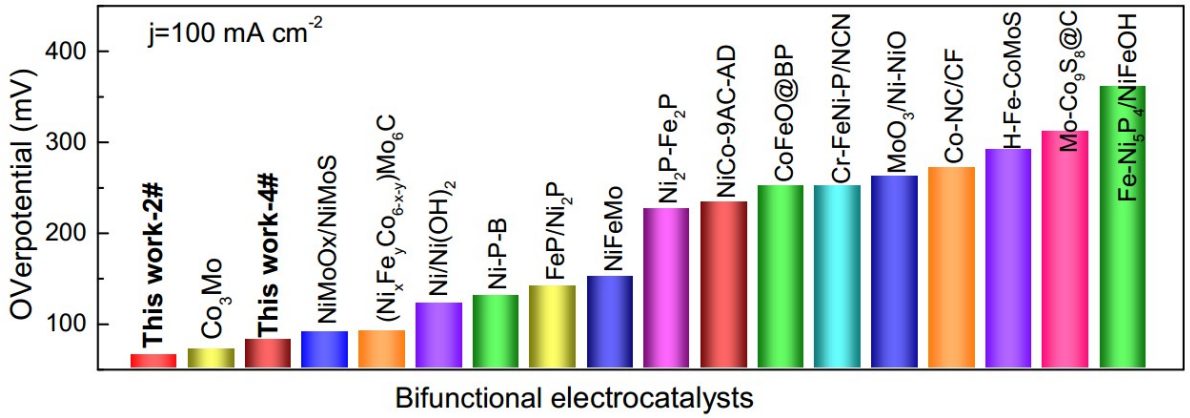

Figure S11. Comparison of the overpotential at 100 mA cm^{-2} for NiMoFe NPs@MoO_2 NPAs with recently reported bifunctional alkaline water splitting catalysts, details can be seen in Table S4.

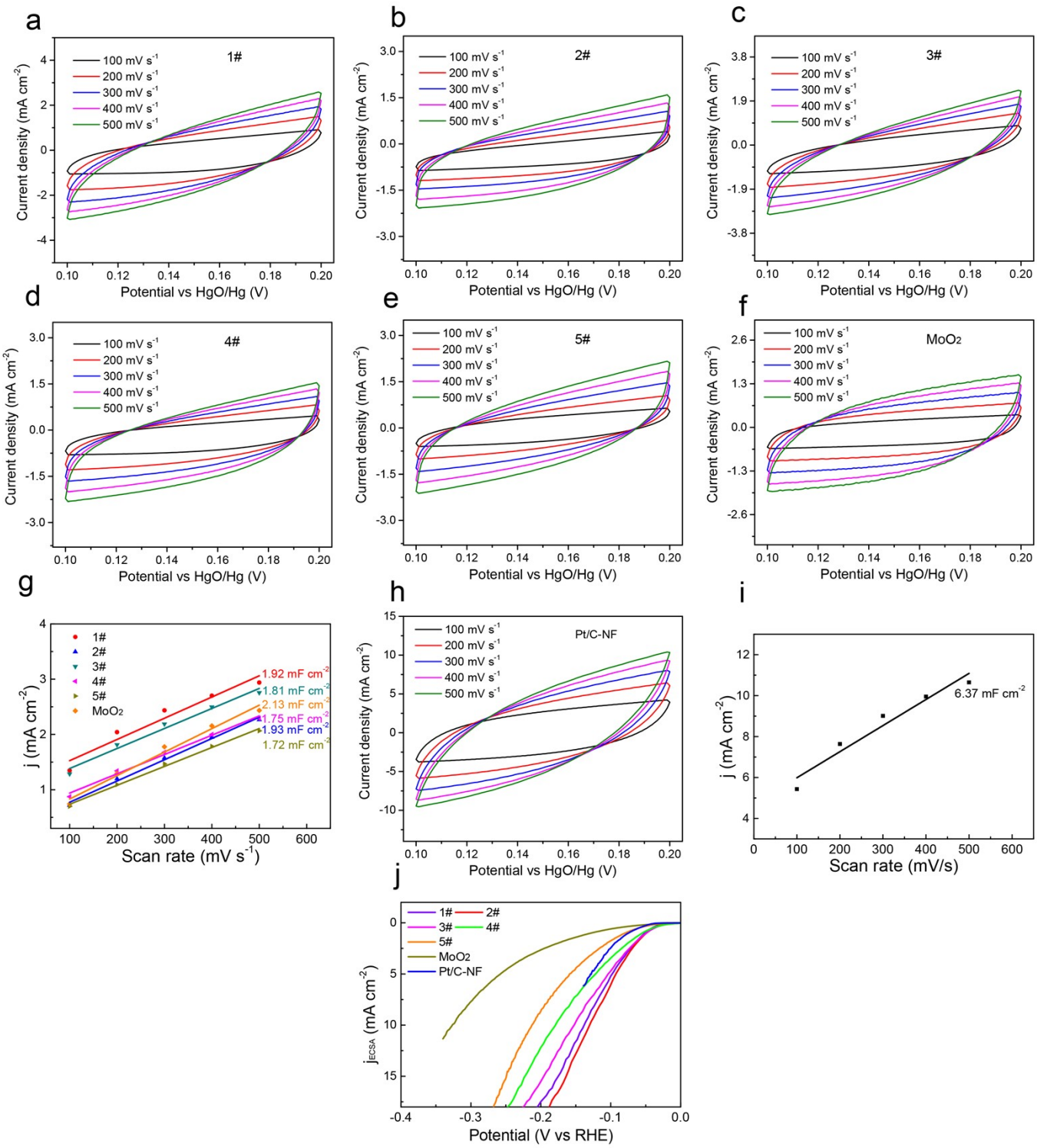

Figure S12. CV curves at different scan rates within a non-Faraday capacitive potential range (a-f) and C_{dl} calculations (g) of 1-5# NiMo(Fe) NPs@MoO_2 NPAs and MoO_2 nano pillar arrays. CV curves at different scan rates within a non-Faraday capacitive potential range (h) and C_{dl} calculations (i) of Pt/C-NF. (j) Electrochemical active surface area (ECSA) normalized HER polarization curves of 1-5# NiMoFe NPs@MoO_2 NPAs, MoO_2 nano pillar arrays and Pt/C-NF.

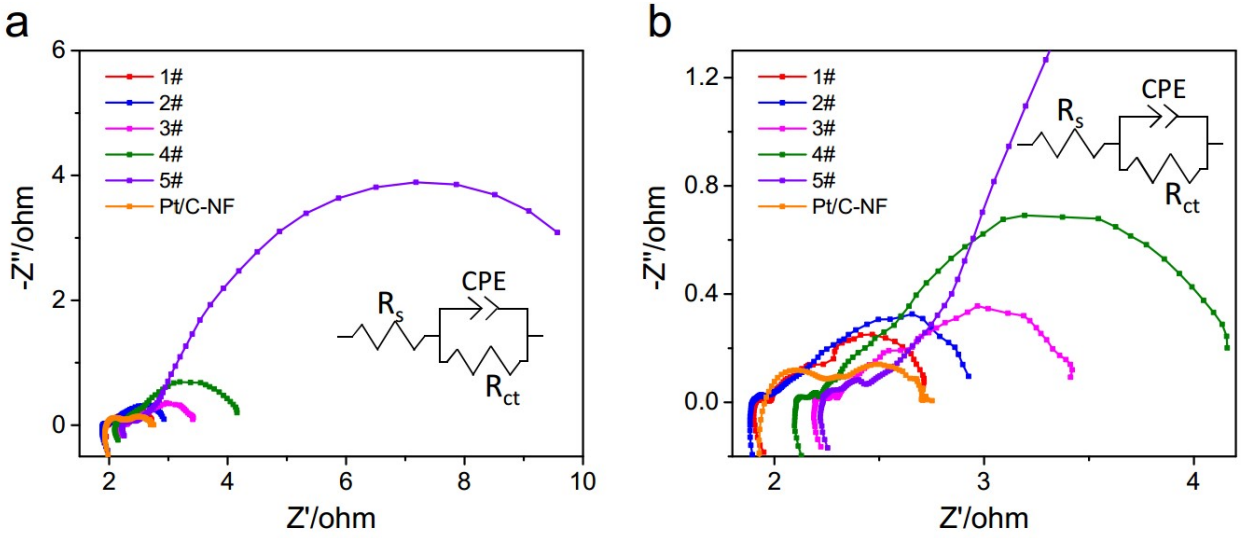

Figure S13. (a) Electrochemical impedance spectroscopy (EIS) of 1-5# NiMoFe NPs@MoO_2 NPAs and Pt/C-NF tested at the overpotential of HER of 100 mV with the same electrode area. (b) Magnification of Figure (a).

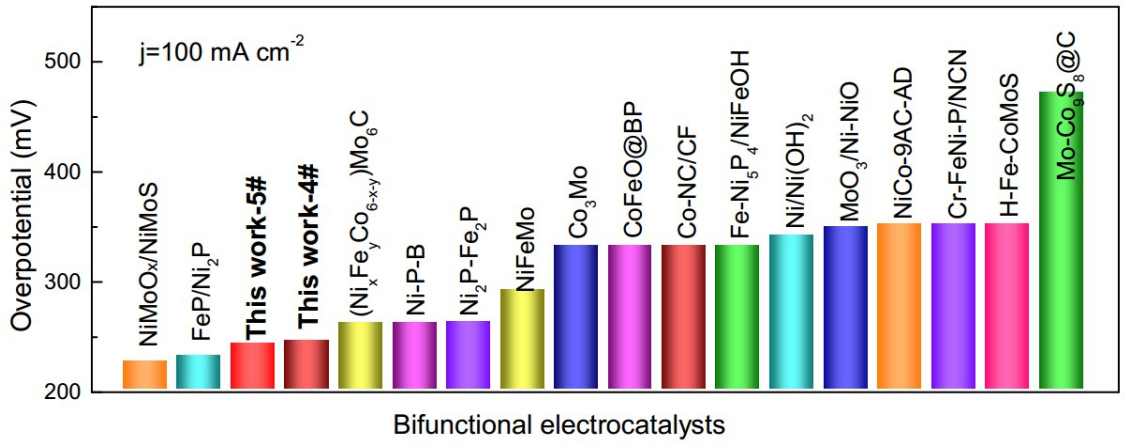

Figure S14. Comparison of the OER overpotential of NiMoFe NPs@MoO_2 NPAs at 100 mA cm^{-2} with recently reported bifunctional alkaline water-splitting catalysts, details can be seen in Table S4.

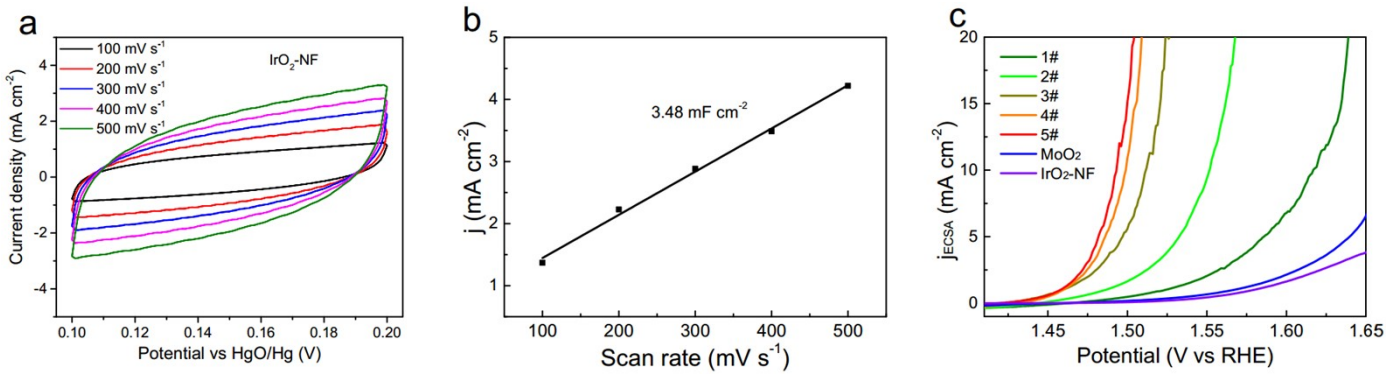

Figure S15. (a) CV curves of IrO_2-NF at different scan rates within a non-Faraday capacitive potential range. (b) C_{dl} calculations of IrO_2-NF. (c) Electrochemical active surface area (ECSA) normalized OER polarization curves of 1-5# NiMoFe NPs@MoO_2 NPAs and IrO_2-NF.

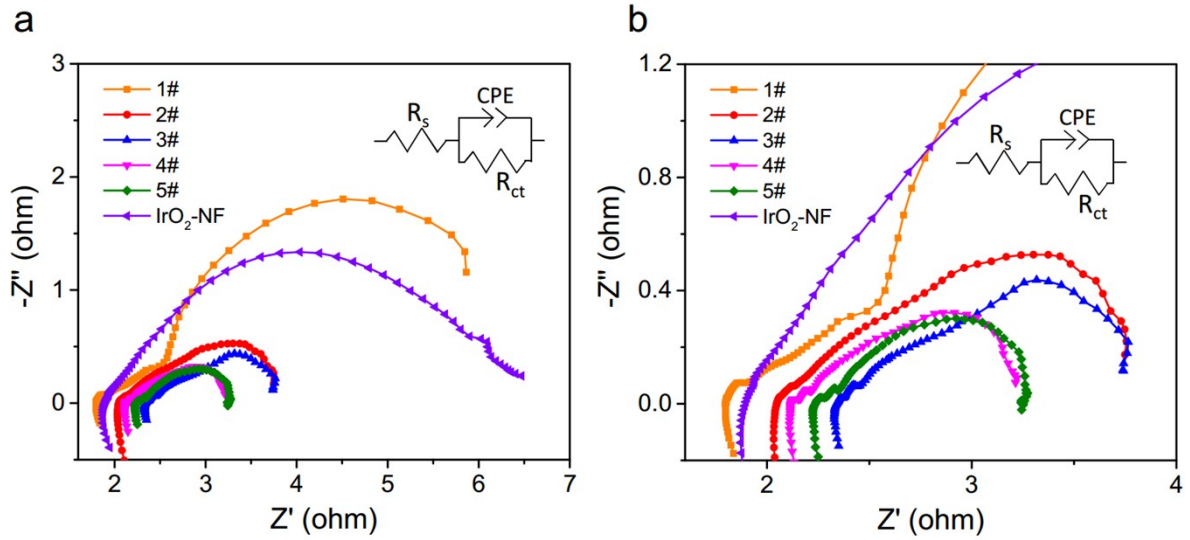

Figure S16. (a) Electrochemical impedance spectroscopy (EIS) of 1-5# NiMoFe NPs@MoO_2 NPAs and IrO_2-NF tested at the overpotential of HER of 100 mV with the same electrode area. (b) Magnification of (a).

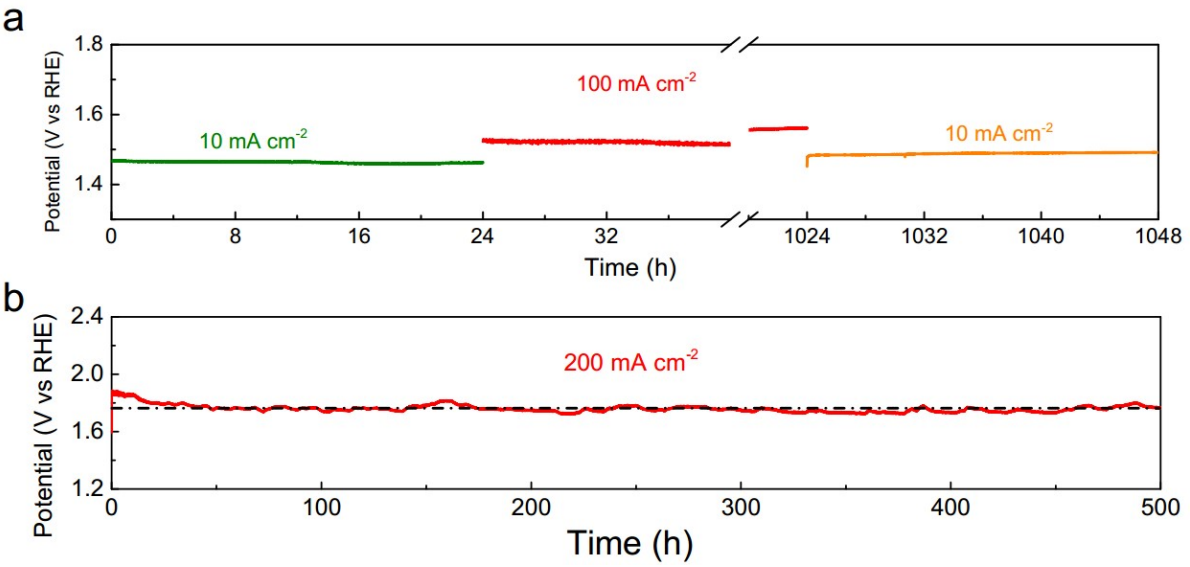

Figure S17. Chronopotential test of 4#||4# NiMoFe NPs@MoO_2 NPAs cell at (a) 10, 100, 10 mA cm^{-2} and (b) 200 mA cm^{-2} in 1.0 M KOH solution at room temperature with iR compensation.

Table S3. HER and OER electrocatalytic performance comparisons among recently reported advanced bifunctional alkaline water-splitting catalysts. η_{10}, η_{100} and η_{200} correspond to the overpotentials at the geometric current densities of 10, 100 and 200 mA cm^{-2}, respectively.

Bifunctional catalysts	HER η_{10} (mV)	HER η_{100} (mV)	HER η_{200} (mV)	HER Tafel (dec^{-1})	OER η_{10} (mV)	OER η_{100} (mV)	OER η_{200} (mV)	OER Tafel (dec^{-1})	Electrolyte	Support	Mass loading (mg cm^{-2})	Reference
NiMoFe@MoO_2-2#	28	67	87	33	224	275	295	64	1 M KOH	Ni foam	39	This work
NiMoFe@MoO_2-4#	28	83	120	40	211	242	252	37	1 M KOH	Ni foam	37	This work
NiMoFe@MoO_2-5#	45	115	155	43	205	239	249	35	1 M KOH	Ni foam	35	This work
Ru–MnFeP	35	~70	-	36	191	~280	~300	69	1 M KOH	Ni foam	NA	Adv. Energy Mater. 2020, 10, 2000814
Mo-Co_9S_8@C	113	~310	-	67.6	200	470	-	95.6	1 M KOH	Carbon paper	1.0	Adv. Energy Mater. 2020, 10, 1903137.
Co-NC/CF	157	~270	~300	109	246	~330	~350	72	1 M KOH	Carbon fiber paper (CFP)	1.1	Energy Environ. Sci., 2020, 13, 545-553
$(Ni_xFe_yCo_{6-x-y})Mo_6C$	20	~90	~130	47.4	212	~260	~280	55.1	1 M KOH	Ni foam	NA	Appl. Catal. B, 290 (2021) 120049
CoFeO@BP	88	250	-	51	266	~330	~390	53	1 M KOH	Black phosphorus	NA	Angew. Chem. Int. Ed. 2020, 59, 21106–21113
Fe-Ni_5P_4/NiFeOH	197	360 (η_{80})	-	94	221	~330 (η_{80})	-	35	1 M KOH	Ni foam	NA	Appl. Catal. B, 291 (2021) 119987
MoO_3/Ni–NiO	62	~260	-	59	-	347	-	60	1 M KOH	carbon cloth	NA	Adv. Mater. 2020, 32, 2003414
Ni_2P-Fe_2P	128	225	~250	86	-	261	~280	58	1 M KOH	Ni foam	15.0	Adv.Funct.Mater. 2021, 31, 2006484.
Cr-doped FeNi–P/NCN	190	250 (η_{70})	-	68.5	240	~350 (η_{80})	-	72.3	1 M KOH	Ni foam	3.0	Adv.Mater. 2019, 31, 1900178.
FeP/Ni_2P	14	~140	-	24.2	154	~230	-	22.7	1 M KOH	Ni foam	8	Nat Commun 9, 2551 (2018)
NiMoOx/NiMoS	38	89	~120	38	186	225	~240	34	1 M KOH	Ni foam	NA	Nat Commun 11, 5462 (2020).
Co_3Mo/Cu	12	~70	~80	40	-	~330	~360	40	1 M KOH and 0.5 M NaCl	Ni foam	NA	Nat Commun 11, 2940 (2020).
Ni-P-B	-	~130	-	42.1	-	~260	-	-	1 M KOH	Ni foam	5.63	Energy Environ. Sci., 2020, 13, 102
Ni/$Ni(OH)_2$	77	~120	-	53	270	~340	-	70	1 M KOH	Carbon papers	0.5	Adv. Mater. 2020, 32, 1906915
Ir-NSG	~18.5	~55 (η_{30})	-	28.3	~256	~290 (η_{30})	-	40	1 M KOH	Carbon fiber paper (CFP)	0.073	Nat Commun 11, 4246 (2020).
$RuTe_2$	34	70 (η_{40})	-	28	275	~390 (η_{50})	-	53	1 M KOH	Glassy carbon electrode	NA	Appl. Catal. B, 278 (2020) 119281
Ir-C≡	7	80 (η_{40})	-	62	300	~340 (η_{40})	-	37	1 M KOH	Glassy carbon electrode	40 μgIr	ACS Catal. 2021, 11, 1179−1188
H–Fe–CoMoS	137	~290	-	98	282	~350	-	58	1 M KOH	Carbon paper	NA	Nano Energy, 2020, 75, 104913
NiFeMo	45	150	200	-	238	290	310	35	1 M KOH	Ni foam	NA	ACS Energy Lett. 2018, 3, 546-554

NiCo-9AC-AD	143	232	-	79.5	-	350	-	51.3	1 M KOH	Ni foam	10.2	ACS Sustainable Chem. Eng. 2019, 7, 21, 18085–18092

Table S4. Full alkaline water splitting performance comparisons among recently reported advanced electrocatalysts (including the non-noble and noble bifunctional catalysts as well as cell couples combined different OER and HER catalysts)**.** V_{10}, V_{100}, V_{200}, V_{500} and V_{1000} correspond to the cell voltages at the geometric current densities of 10, 100, 200, 500 and 1000 mA cm^{-2}, respectively.

Bifunctional catalysts	V_{10}	V_{100}	V_{200}	V_{500}	V_{1000}	Water splitting stability	Electrolyte	Support	Mass loading (mg cm^{-2})	Reference
NiMoFe@MoO_2-4#	1.46	1.52	1.56	1.61	1.66	1000 h@100 mA cm^{-2} 500 h@200 mA cm^{-2}	1 M KOH	Ni foam	37	This work
Ir-NSG	1.45	~1.57	~1.62	~2.15	~2.3	24 h@10 mA cm^{-2}	1 M KOH	Carbon fiber paper	0.073	Nat Commun 11, 4246 (2020).
FeP/Ni_2P	1.42	~1.6	/	1.72	/	40 h@500 mA cm^{-2}	1 M KOH	Ni foam	8	Nat Commun 9, 2551 (2018)
$NiMoO_x$/NiMoS	1.46	1.62	~1.67	1.75	1.82	500 h@500 mA cm^{-2}	1 M KOH	Ni foam	NA	Nat Commun 11, 5462 (2020).
Co_3Mo/Cu	/	1.62	~1.67	/	/	30 h@145 mA cm^{-2}	1 M KOH and 0.5 M NaCl	Ni foam	NA	Nat Commun 11, 2940 (2020).
Graphene/MoS_2/FeCoNi$(OH)_x$ (+)//Graphene/MoS_2/FeCoNiPx (−)	/	1.59	1.65	1.76	/	100 h@100 mA cm^{-2} 100 h@50 mA cm^{-2}	1 M KOH	Carbon fiber	6.7 5.9	Nat Commun 12, 1380 (2021).
MoO3/Ni–NiO	1.55	~1.78 (η80)	/	/	/	20 h@10 mA cm^{-2}	1 M KOH	Carbon cloth	NA	Adv. Mater. 2020, 32, 2003414
Cr-doped FeNi–P/NCN	1.50	~1.69	/	/	/	20 h@10 mA cm^{-2}	1 M KOH	Ni foam	3.0	Adv. Mater. 2019, 31, 1900178.
Ni/$Ni(OH)_2$	1.59	1.70 (η60)	/	/	/	20 h@10 mA cm^{-2}	1 M KOH	Carbon papers	0.5	Adv. Mater. 2020, 32, 1906915
Ni-P-B	/	1.68	1.72	/	/	240 h@1000 mA cm^{-2}	1 M KOH	Ni foam	5.63	Energy Environ. Sci., 2020, 13, 102
Ni nanowire array(-)//$Ni_{0.8}Fe_{0.2}$-AHNA(+)	1.41	1.545	~1.61	1.702	1.76	24 h@500 mA cm^{-2}	1 M KOH	Ni foam	2.5	Energy Environ. Sci., 2020, 13, 86-95
Co-NC/CF	1.65	1.86	~1.9	/	/	100 h@20 mA cm^{-2}	1 M KOH	Carbon fiber paper	1.1	Energy Environ. Sci., 2020, 13, 545-553
CoFeO@BP	1.58	~1.77	~1.82	/	/	24 h@10 mA cm^{-2}	1 M KOH	Black phosphorus	NA	Angew. Chem. Int. Ed. 2020, 59, 21106–21113
Ru–MnFeP	1.47	~1.62	~1.72	/	/	50 h@20 mA cm^{-2}	1 M KOH	Ni foam	NA	Adv. Energy Mater. 2020, 10, 2000814
Mo-Co_9S_8@C	1.56	1.96 (η50)	/	/	/	72 h@10 mA cm^{-2}	1 M KOH	Carbon paper	1.0	Adv. Energy Mater. 2020, 10, 1903137.
Ir-C≡	1.50	~1.57	/	/	/	20 h@10 mA cm^{-2}	1 M KOH	Glassy carbon electrode	40 μgIr	ACS Catal. 2021, 11, 1179−1188
Ni_2P-Fe_2P	/	1.682	~1.74	1.865	~1.95	48 h@100 mA cm^{-2} 42 h@500 mA cm^{-2}	1 M KOH	Ni foam	15.0	Adv. Funct. Mater. 2021, 31, 2006484.
$RuTe_2$	1.57	~2.0	/	/	/	20 h@10 mA cm^{-2}	1 M KOH	Glassy carbon electrode	NA	Appl. Catal. B, 278 (2020) 119281

$(Ni_xFe_yCo_{6-x-y})Mo_6C$	1.47	~1.60	1.69	1.77	~1.86	50 h@500 mA cm^{-2}	1 M KOH	Ni foam	NA	Appl. Catal. B 290 (2021) 120049
Fe-Ni_5P_4/NiFeOH	1.55	~1.56	/	/	/	20 h@10 mA cm^{-2}	1 M KOH	Ni foam	NA	Appl. Catal. B 291 (2021) 119987
H–Fe–CoMoS	1.50	1.80 (η80)	/	/	□	10 h@20 mA cm^{-2}	1 M KOH	Carbon papers	NA	Nano Energy, 2020, 75, 104913
NiFeMo	1.45	1.82	/	/	/	50 h@25 mA cm^{-2}	1 M KOH	Ni foam	NA	ACS Energy Lett. 2018, 3, 546-554
NiCo-9AC-AD	1.56	~1.71	/	/	/	30 h@10 mA cm^{-2}	1 M KOH	Ni foam	10.2	ACS Sustainable Chem. Eng. 2019, 7, 21, 18085–18092

* Note: The blue-marked two cell couples combined different OER and HER catalysts as the anode and cathode. Part of the data shown in the table was measured from the graph in the references and marked by the symbol of "~".

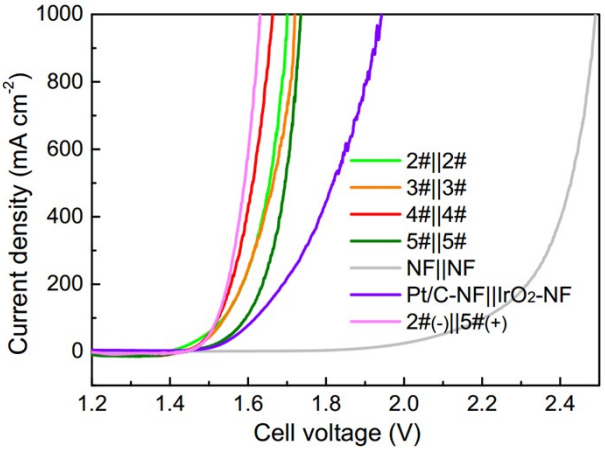

Figure S18. Full water splitting polarization curves of NiMoFe NPs@MoO_2 NPAs with different compositions and pure nickel foam as electrodes, and commercial Pt/C and IrO_2 on NF recorded in 1 M KOH (iR-corrected).

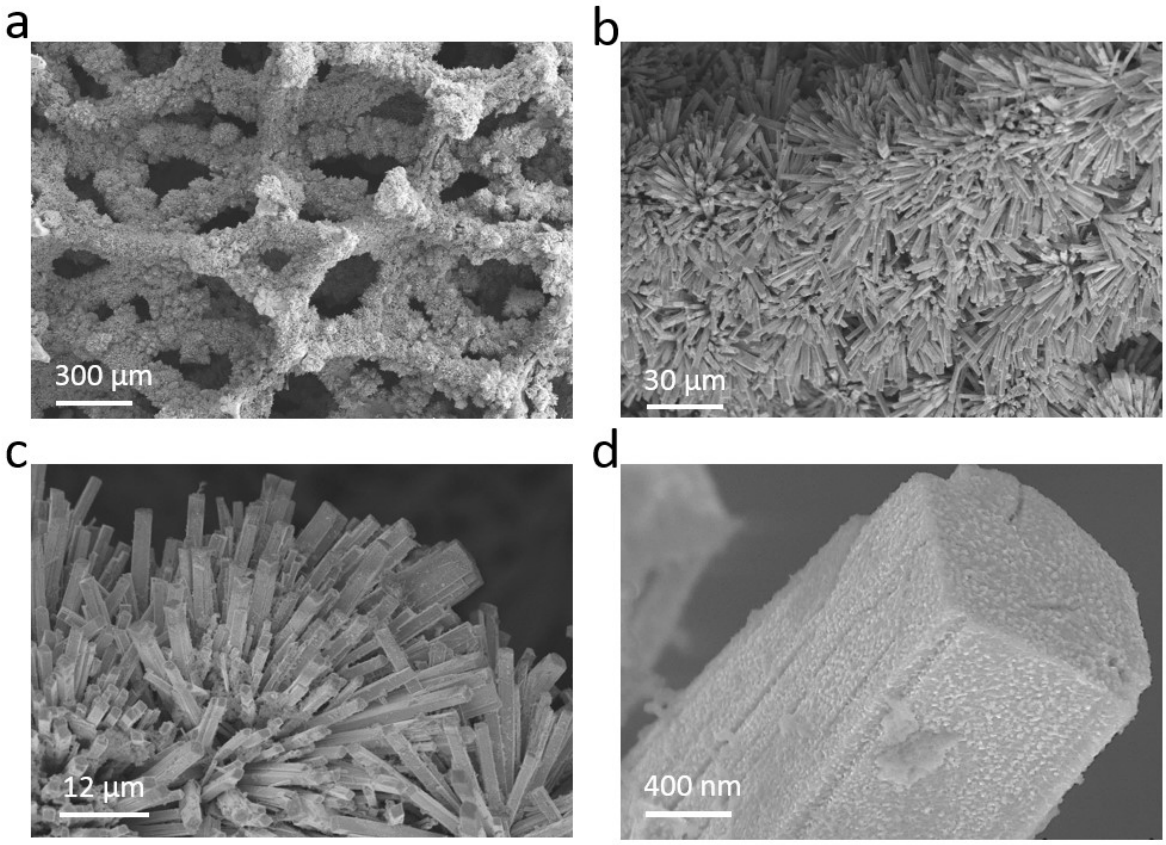

Figure S19. (a-d) SEM images of 4#-NiMoFe NPs@MoO_2 NPAs after 1048-h water splitting test at 10, 100 and 10 mA cm^{-2} as the cathode in 1.0 M KOH solution at room temperature.

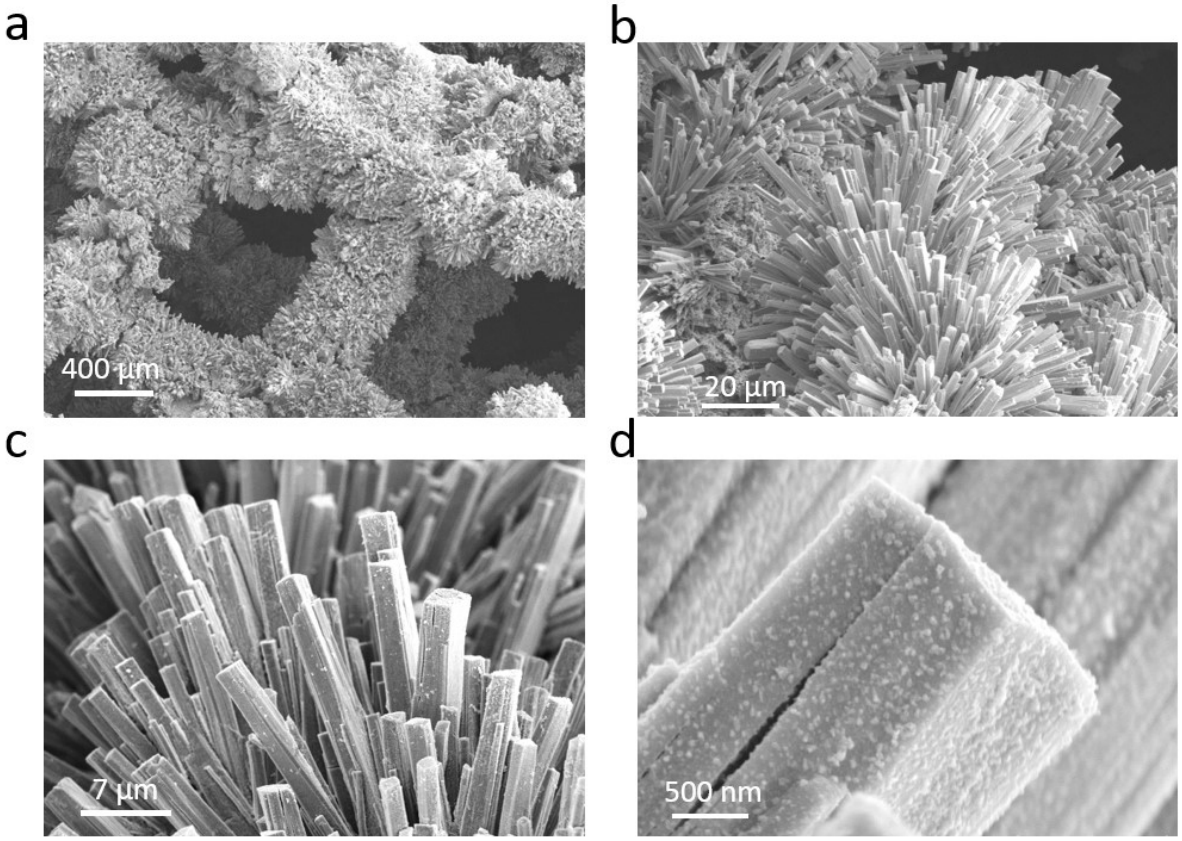

Figure S20. (a-d) SEM images of 4#-NiMoFe NPs@MoO_2 NPAs after 1048-h water splitting test at 10, 100 and 10 mA cm^{-2} as the anode in 1.0 M KOH solution at room temperature.

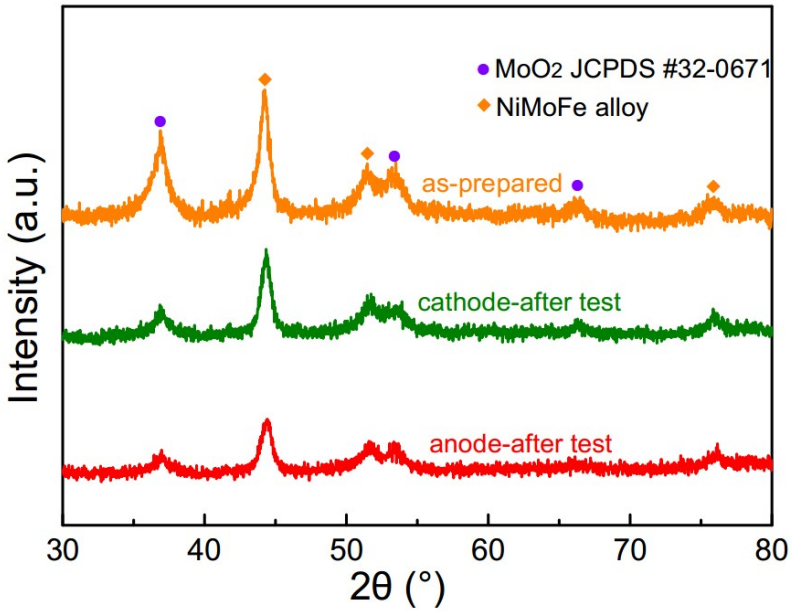

Figure S21. XRD patterns of the 4#-NiMoFe NPs@MoO_2 NPAs-NF before and after 1048-h water splitting test at 10, 100 and 10 mA cm^{-2} as a bifunctional catalyst in 1.0 M KOH solution at room temperature.

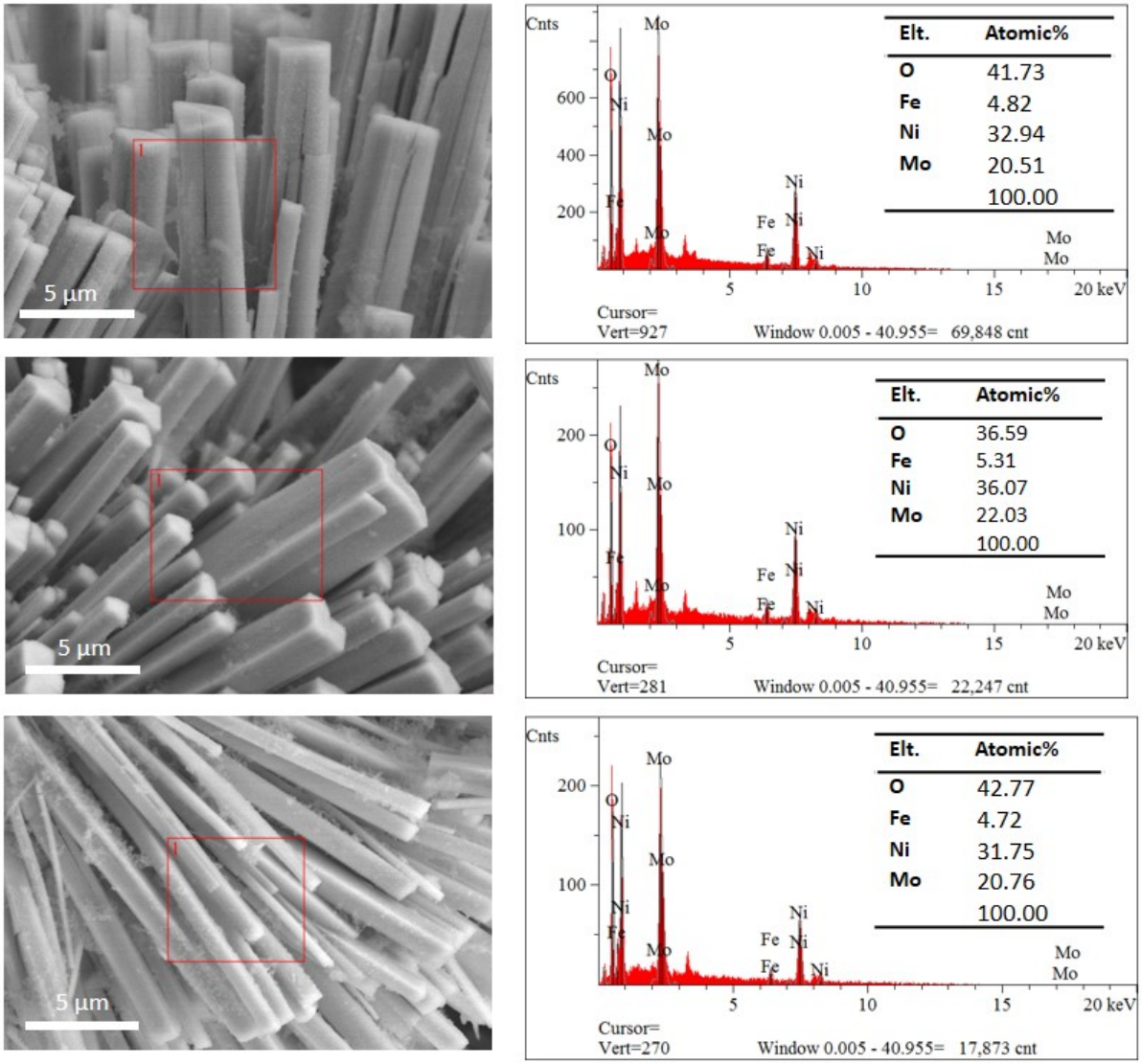

Figure S22. SEM images and corresponding EDS analysis of 4#-NiMoFe NPs@MoO_2 NPAs after 1048-h water splitting test at 10, 100 and 10 mA cm^{-2} as the cathode in 1.0 M KOH solution at room temperature.

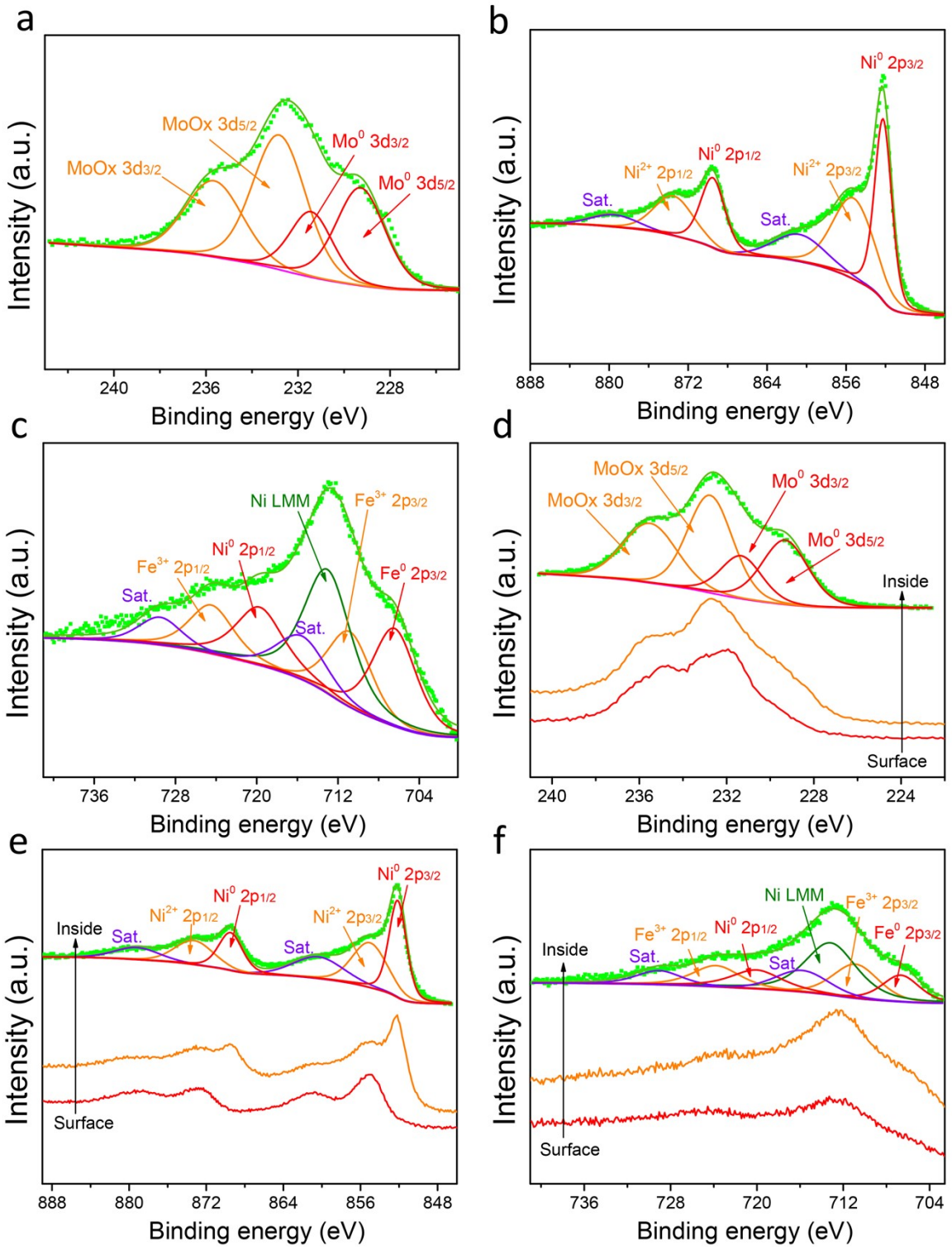

Figure S23. High-resolution XPS spectra of Mo 3d (a), Ni 2p (b), and Fe 2p (c) for 4# NiMoFe NPs@MoO_2 NPAs as anode after 1024-h test with 3-min argon ion bombardment (15 nm). High-resolution XPS spectra (depth profile) of Mo 3d (d), Ni 2p (e), and Fe 2p (f) for 4# NiMoFe NPs@MoO_2 NPAs after 1-hour 10-mA cm^{-2} OER test with 0, 1.5, 3-min argon ion bombardment (surface, 8 nm, 15 nm).

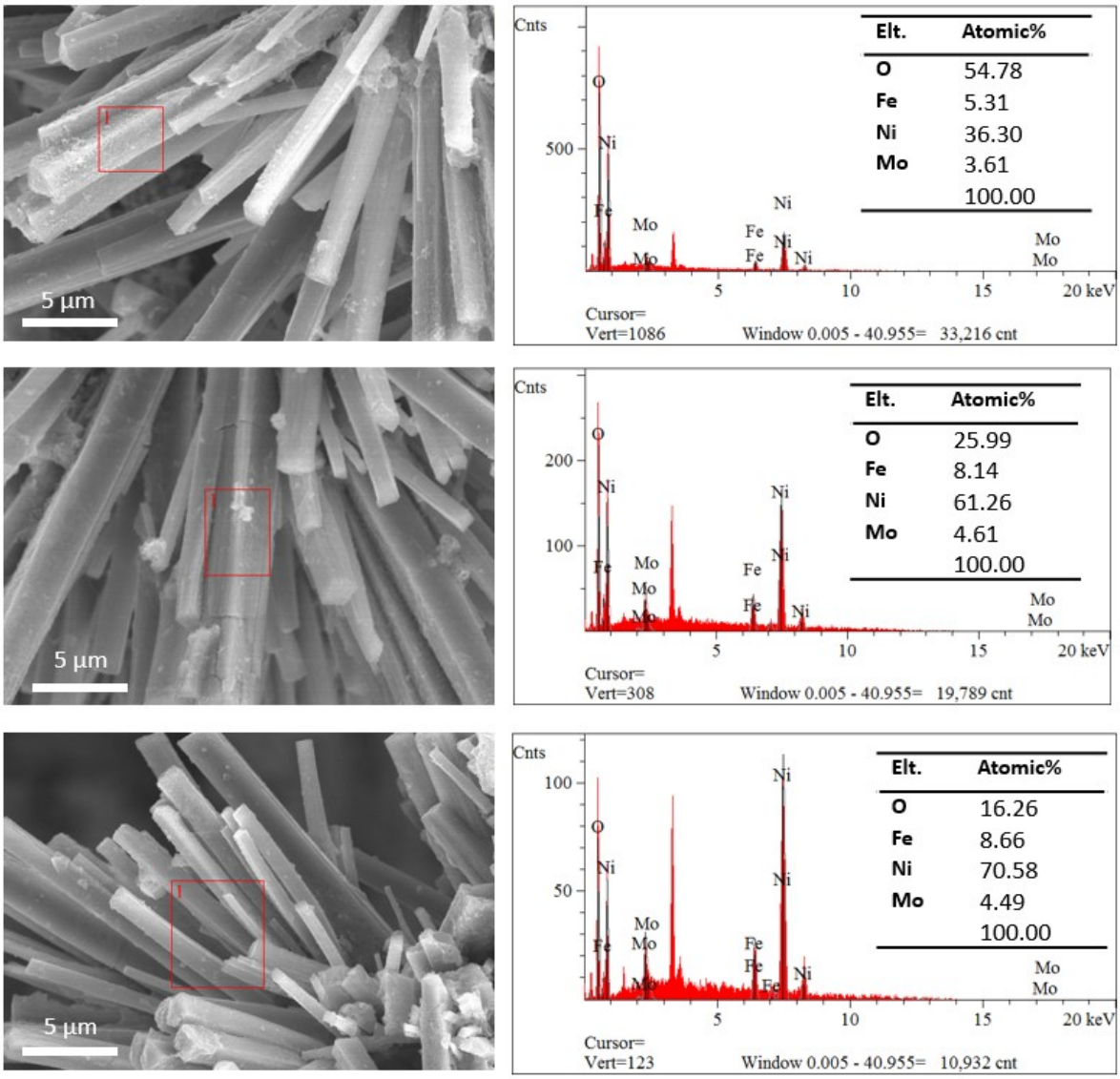

Figure S24. (a-c) SEM images and corresponding EDS analysis of 4#-NiMoFe NPs@MoO_2 NPAs after 1048-h water splitting test at 10, 100 and 10 mA cm^{-2} as the anode in 1.0 M KOH solution at room temperature.

Table S5. Summary of SEM EDS results of 4# NiMoFe NPs@MoO_2 NPAs from Figure S3, S20 and S21.

Elements	as-prepared (at %)	after testing-cathode (at %)	after testing-anode (at %)
O	37.7	40.4	32.3
Fe	3.0	5.0	7.4
Ni	25.5	33.6	56.0
Mo	33.8	21.1	4.2

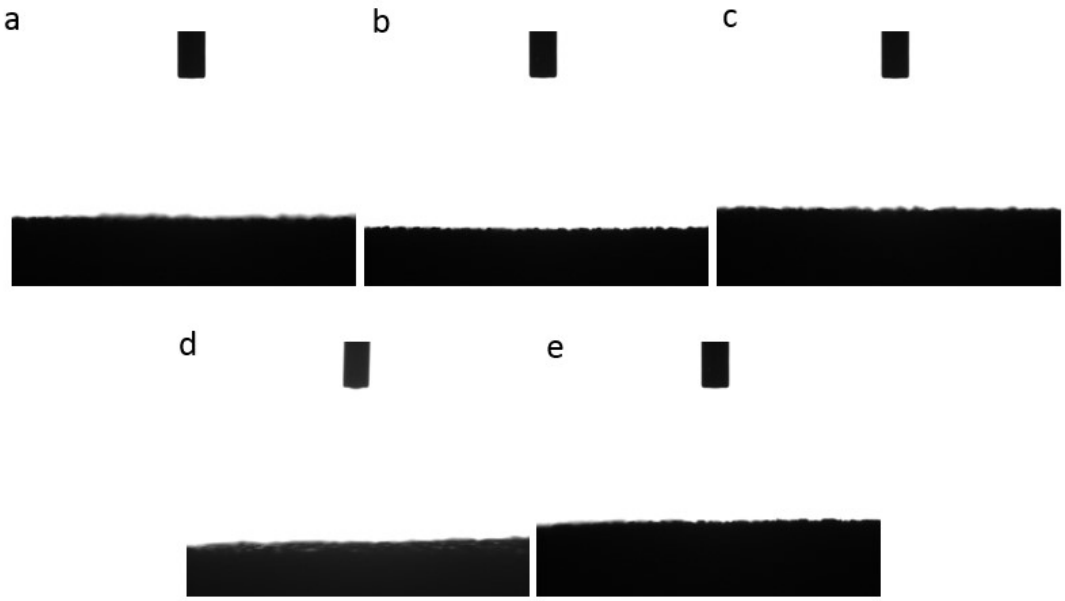

Figure S25. Optical images showing the static water contact angles (θ) of 1-5# NiMo(Fe) NPs @MoO_2 NPAs (a-e).

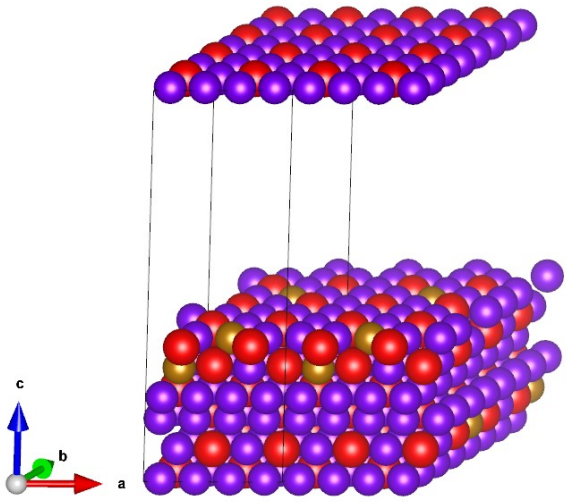

Figure S26. Schematic of the NiMoFe model. The supercell is marked by the black box (purple: Ni; gold: Fe; red: Mo).

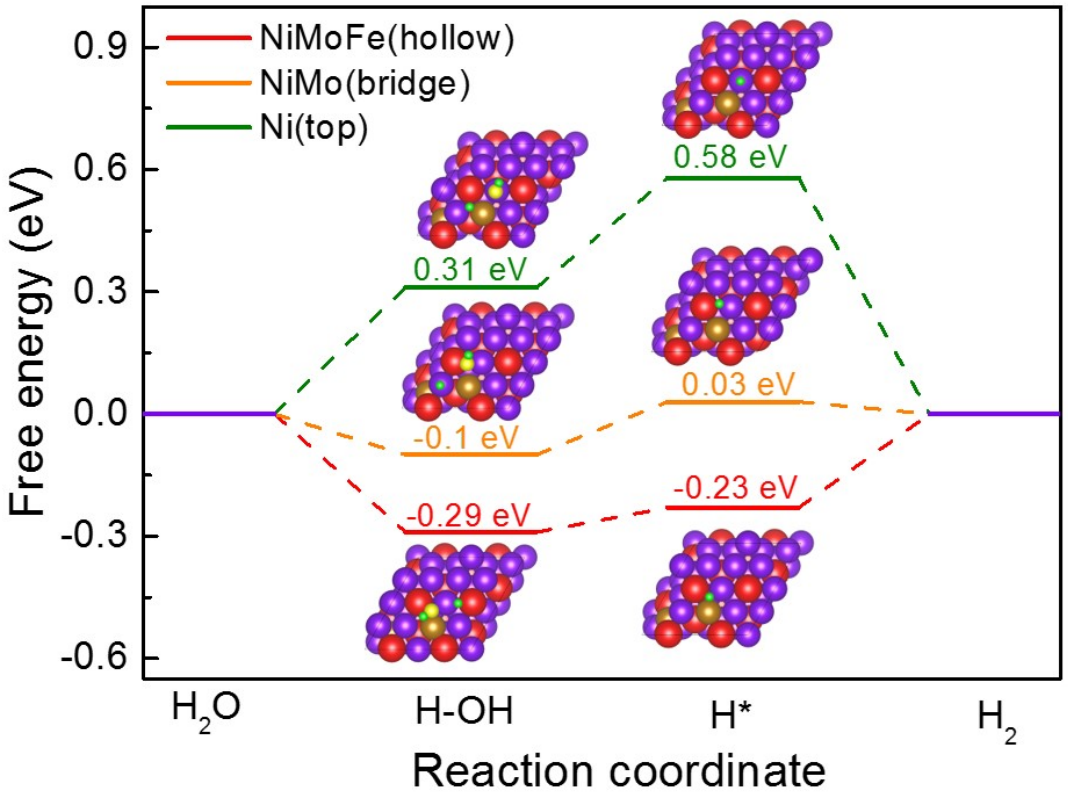

Figure S27. The free energy diagram for alkaline HER on different reaction sites of NiMoFe alloy. The adsorption sites of the intermediates OH-H and H* are shown in the inset. (purple: Ni; gold: Fe; red: Mo; green: H; yellow: O).

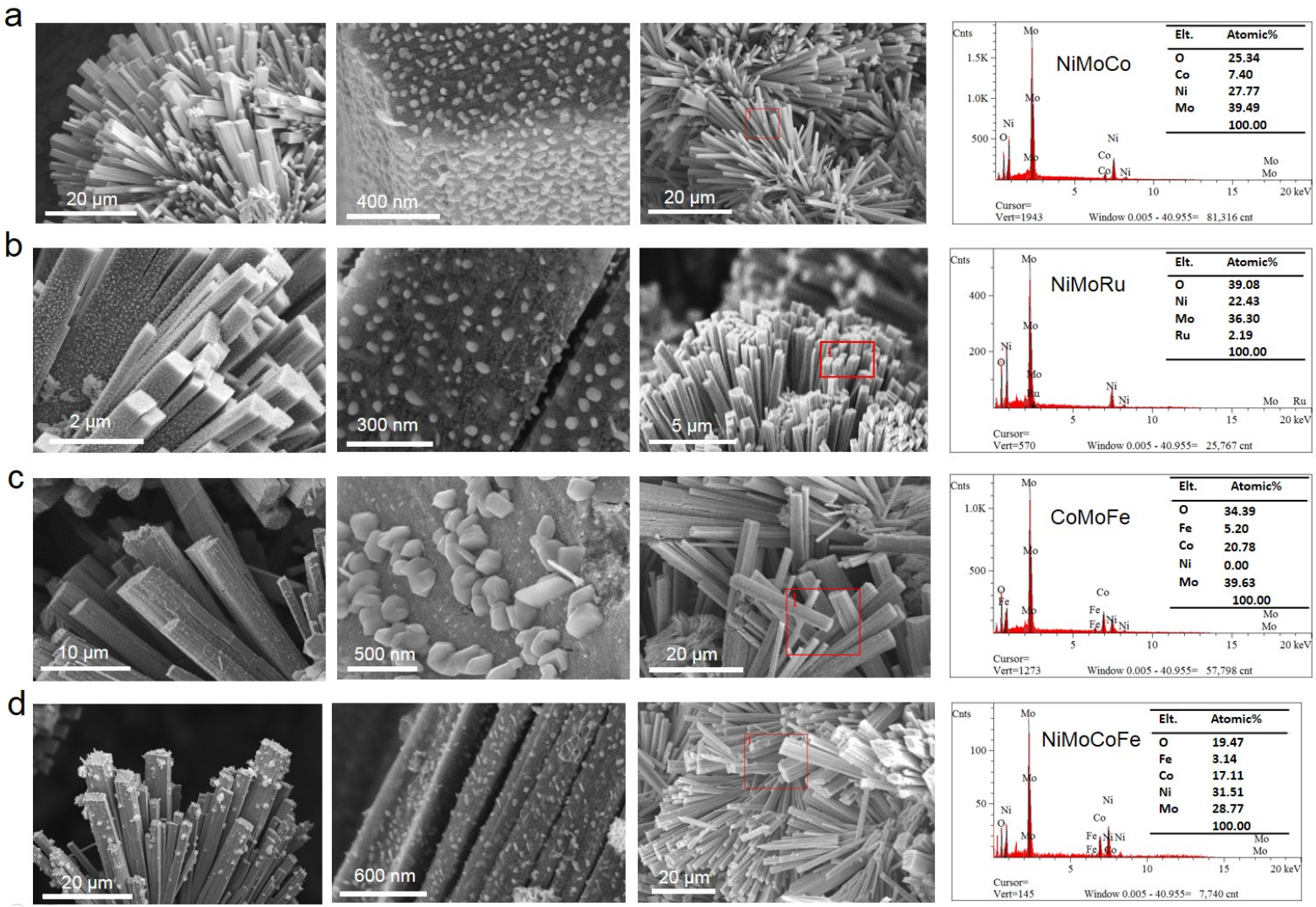

Figure S28. SEM images and corresponding EDS analysis of (a) NiMoCo, (b) NiMoRu, (c) CoMoFe and (d) NiMoCoFe NPs@MoO_2 NPAs prepared by the reductive annealing-induced phase separation method.

References:

[1] a) G. Kresse, J. Furthmüller, *Physical Review B* **1996**, 54, 11169; b) G. Kresse, J. Hafner, *Physical Review B* **1994**, 49, 14251.
[2] P. E. Blöchl, *Physical Review B* **1994**, 50, 17953.
[3] a) J. P. Perdew, K. Burke, M. Ernzerhof, *Physical Review Letters* **1996**, 77, 3865; b) Y. Zhang, W. Yang, *Physical Review Letters* **1998**, 80, 890; c) B. Hammer, L. B. Hansen, J. K. Nørskov, *Physical Review B* **1999**, 59, 7413.
[4] H. J. Monkhorst, J. D. Pack, *Physical review B* **1976**, 13, 5188.